DISSERTATION

TWO-DIMENSIONAL OXYGEN CLUSTERS

AND

FILMS ADSORBED ON GRAPHITE

Submitted by

Ru-Pin Chao Pan

Department of Physics

In partial fulfillment of the requirements

for the Degree of Doctor of Philosophy

Colorado State University

Fort Collins, Colorado

Jaunary 1981

COLORADO STATE UNIVERSITY

January 19 81

WE HEREBY RECOMMEND THAT THE DISSERTATION PREPARED UNDER OUR SUPERVISION BY RU-PIN CHAO PAN

ENTITLED TWO-DIMENSIONAL OXYGEN CLUSTERS AND FILMS ADSORBED ON GRAPHITE

BE ACCEPTED AS FULFILLING IN PART REQUIREMENTS FOR THE DEGREE OF DOCTOR OF PHILOSOPHY

Committee on Graduate Work

Nelson S. Gillis

Gearold R. Johnston

James R. Sites

Richard D. Ellers

Adviser

ABSTRACT OF DISSERTATION

TWO-DIMENSIONAL OXYGEN CLUSTERS AND FILMS ADSORBED ON GRAPHITE

The orientations, structures and phase transitions of two-dimensional oxygen molecular clusters adsorbed on the graphite plane were studied using the Monte-Carlo method. Orientational phase transitions have been found for all cluster sizes studied. Melting temperatures show agreement with measured values for extremely low coverage films.

Two different approximations were used in the cluster studies. In one approximation, the interaction between a cluster and the surface was ignored and the center of mass of each oxygen molecule was fixed on a plane. In the other case an atom-atom Lennard-Jones potential was used to determine the surface interaction. An analytic expression was used for the summation over all the carbon atoms in the graphite.

The minimal energies and structures of infinite adsorbed films were studied using an energy minimization method. Two stable phases have been found. The molecules in the low density phase are all oriented parallel to the substrate, while the molecules in the high density phase are perpendicular to the substrate. These two phases are identified as the experimentally measured δ and β phases, respectively. The lattice constants are found to be in agreement with the measured values within 3%.

Ru-Pin Chao Pan
Department of Physics
Colorado State University
Fort Collins, Colorado 80523
January 1981

ACKNOWLEDGEMENTS

It is a distinct pleasure for me to acknowledge the assistance and friendship of my advisors, Dr. Richard D. Etters and Dr. James R. Sites, who in their individual and different ways made my stay at Colorado State University possible both as a student and as an individual.

I would like to thank Dr. Nelson S. Gillis and Dr. Gearold R. Johnson for serving on my committee, Mr. Roy Palmer of NASA Lewis Computer Service Division for considerable help in programming, and Dr. Charles R. Fuselier for many discussions. The financial support of the State of Colorado and the National Aeronautics and Space Administration is deeply appreciated.

I am grateful for the encouragement and patience shown by my husband, Ci-Ling, who as a scientist himself, offered many good suggestions in this work.

TABLE OF CONTENTS

LIST OF FIGURES

LIST OF FIGURES (continued)

LIST OF FIGURES (continued)

CHAPTER I

INTRODUCTION

Absorbed films on the graphite basal plane have been studied intensively since forms of graphite with large amounts of smooth and uniformly oriented surface planes, e.g. Grafoil have become available. As a substrate material, graphite is ideal because it always provides a cleaved surface due to the weak bonding between the layers of carbon atoms. In addition, the interatomic distance among the carbon atoms (1.42 Å) of graphite is much smaller than the sizes of typical adsorbent atoms and molecules studied (3 to 4 Å). Therefore, graphite can be considered as having a smooth surface. These adsorbed films are known to exist in solid, liquid, and vapor phases and undergo phase transitions just as the three-dimensional systems. Some of these adsorbed films, e.g., N_2[1], are commensurate with the substrate while others like O_2[2] are incommensurate with the graphite lattice. Some films such as Kr on graphite undergo phase transition from a registered to nonregistered phase[3] (Fig. I-1). The nature of this transition has been discussed theoretically for absorbed rare gas films.[4] The Ar film does not register to the substrate, but the orientation of the film with respect to graphite lattice changes with its lattice constant. This effect has been observed by low energy electron diffraction measurements.[5] The cause for this orientational epitaxy has been discussed by Novaco and McTague using static distortion wave theory[6] and by Fuselier who minimized the film-surface energy.[7] Pair-wise atom-atom potentials were used for the Ar-Ar and Ar-C interactions in both works.

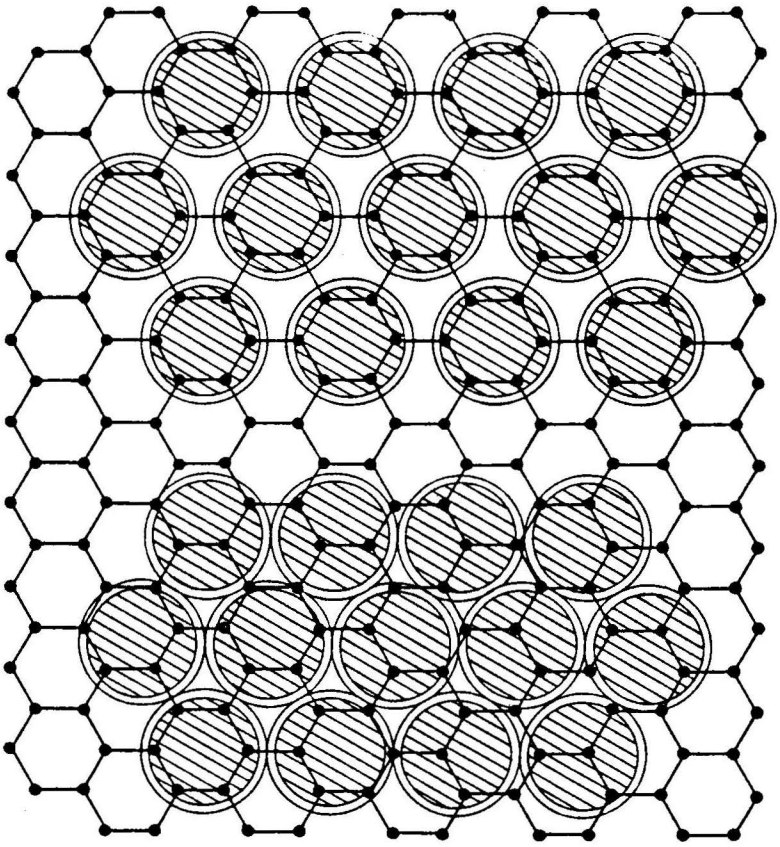

Figure I-1. Schematic representation of the $\sqrt{3} \times \sqrt{3}$ registered phase (top) and the incommensurate Ar monolayer phase (bottom). The hexagons represent the graphite lattice with C-atoms sitting on the vertexes. The circles represent the adsorbed atoms.

Both theoretical and experimental studies[1-7] on the thermodynamic, structural and dynamic properties of these adsorbed systems have greatly increased our knowledge of physical adsorption and of the condensed phase of ideal two-dimensional systems. Studies for adsorbed polyatomic molecules can reveal even more information about the surface field and the anisotropy of molecular interactions. The O_2 system receives much attention because its bulk α-phase is the only known homonuclear antiferromagnetic insulator. Recently, the structures and the phase transitions of the adsorbed oxygen films have been studied by neutron scattering,[2] specific heat measurements,[8,9] and x-ray scattering.[10] Three solid film phases have been found, i.e., the α , β and δ phases, as named by Nielson and McTague.[2] The α region is an anti-ferromagnetic phase and corresponds to anti-ferromagnetic bulk O_2 . The paramagnetic β region corresponds to β bulk O_2 . The δ phase has a face-centered rectangular lattice with oxygen molecules parallel to the substrate and along the longer side of the lattice rectangles.[10] The α and β structures are almost identical to the closest packed (a-b) plane structures of bulk α and β oxygen respectively, the structures of which are shown in Fig. I-2. These two phases have the same density and the molecules are all perpendicular to the substrate. The β phase is in a triangular lattice, while the α phase is distorted into an isosceles triangular lattice with long range antiferromagnetism. No registry to the substrate has been detected. A phase diagram has been partially mapped out[2] and is shown in Fig. I-3. The coverage or filling, i.e., the number of O_2 molecules per unit area, ρ , is scaled so that the

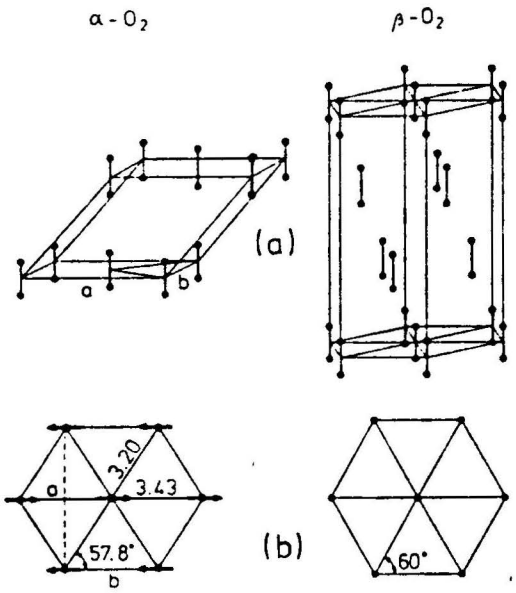

Figure I-2. (a) Structures of bulk α and β O_2. (b) Structures of the densest packed planes of bulk α and β O_2. Arrows indicate the directions of spin.

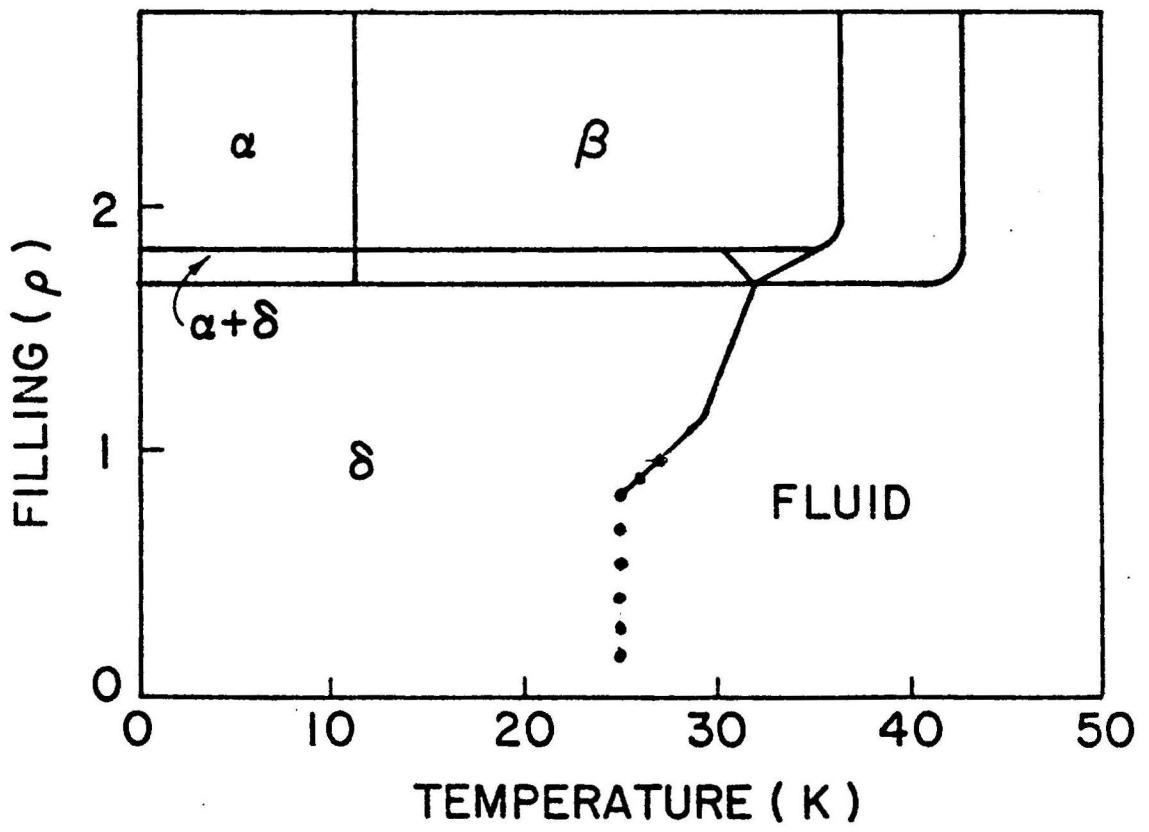

Figure I-3. Phase diagram for O_2 adsorbed on Grafoil. The α, β and δ phases are solid and the lines refer to phase boundaries.

well-known $\sqrt{3} \times \sqrt{3}$ commensurate structure (Fig. I-1) corresponds to unity. The dots are results of specific heat measurements.[8]

In this work, we have developed several physical models and applied them to the study of the equilibrium configurations and thermodynamic properties of adsorbed oxygen on graphite. In particular, a cluster model is proposed to study the low density region, for which very little information is available. Three dimensional clusters have been found during vapor nucleation,[11] in rare gas supersonic beams[12] and in many other situations.[13] The nucleation of adsorbed rare gas films on a graphite basal plane has been studied experimentally and interpreted using a two-dimensional cluster model.[14] Microclusters of rare gas atoms in two dimensions and adsorbed on surfaces have been studied by using molecular dynamics.[15] This model seems a reasonable approach to study the nucleation of a film or the thermodynamic properties of the adsorbed film at extremely low density, i.e., $\rho << 1$. In this work, the structures and phase transitions of two-dimensional oxygen clusters with N ranging from 2 to 12 molecules adsorbed on graphite basal plane surface were studied by the Monte-Carlo method.

Two different approximations were made. In the first case, interactions between oxygen molecules and graphite were ignored but the O_2 molecular centers were constrained to a plane. This approximation is based upon the neutron scattering measurements[2] showing that α and β films have structures almost identical to the a-b plane structures of bulk α and β O_2, with no registry. The molecules have the freedom to move along the plane and to rotate. In a second approximation, the two-dimensional constraint was removed and

an atom-atom potential between oxygen and graphite was used. It is assumed that the graphite structure is not altered by temperature change, or by the presence of O_2 molecules. It is also assumed that the atoms in the graphite are stationary.

An atom-atom Lennard-Jones potential with quadrupolar interactions between O_2 molecule pairs was used. This was suggested first by English and Venables, who successfully predicted the β-phase structure of solid oxygen.[16] The α-phase structure is similar to but distorted from the β -phase structure. To explain this distortion, the spin interaction has to be considered, because O_2 has spin 1 and the α-phase oxygen is an antiferromagnetic system.[17] Using the orbital overlapping method, English[18] was able to explain the α-phase structure but there remains a big discrepancy quantitatively. It seems that the antiferromagnetic coupling constant drops so fast that it is beyond the prediction of any simple approximation. In our study, the spin interactions have been ignored. We feel that more accurate information about the spin interaction between oxygen molecules is necessary to predict any magnetic property in the cluster systems.

The energies and structures of the adsorbed infinite films have been studied with energy minimization method. The particular technique we applied was the "pattern search" method. Both the atom-atom Lennard-Jones potential and the isotropic Lennard-Jones potentials for oxygen molecule have been used for the surface interaction. The energy per unit area as a function of film density has been plotted for each case. From the minima of these curves, the stable configurations of the film have been found.

CHAPTER II

INTERACTION

Consider a system of O_2 molecules adsorbed on a graphite substrate. The total potential energy E consists of three parts, i.e.,

$$E = V_1 + V_2 + V_3 \tag{II-1}$$

where V_1 is the internal energy among the adsorbed oxygen molecules, assuming that the bond length in a O_2 molecule is not perturbed. V_2 is the adsorption energy, which is the interaction energy between the adsorbed molecules and the graphite, and V_3 is the internal energy of graphite solid. It is assumed that the graphite structure is not perturbed by temperature, or by the presence of oxygen and that the atoms in graphite are stationary. Therefore V_3 is a constant, which can be ignored. Assuming only two body interaction, V_1 can be written as

$$V_1 = \sum_{i<j} V_{O_2-O_2}(\vec{r}_i, \vec{\omega}_i, \vec{r}_j, \vec{\omega}_j) , \tag{II-2}$$

where $V_{O_2-O_2}$ is the potential energy between molecules i and j, located at $\vec{r}_i$ and $\vec{r}_j$, with orientations $\vec{\omega}_i$ and $\vec{\omega}_j$, respectively. An atom-atom Lennard-Jones potential, with a quadrupolar interaction is used for $V_{O_2-O_2}$ i.e.,

$$V_{O_2\text{-}O_2}(\vec{r}_1, \vec{\omega}_1, \vec{r}_2, \vec{\omega}_2) = \sum_{i=1}^{4} 4\varepsilon\left(\left(\frac{\sigma}{r_i}\right)^{12} - \left(\frac{\sigma}{r_i}\right)^{6}\right)$$

$$+ \frac{Q^2}{R^5}\Big[6P_2^o(\cos\theta_1)P_2^o(\cos\theta_2)$$

$$- \frac{4}{3} P_2^1(\cos\theta_1)P_2^1(\cos\theta_2)\cos\phi_{12}$$

$$+ \frac{1}{12} P_2^2(\cos\theta_1)P_2^2(\cos\theta_2)\cos\phi_{12}\Big], \qquad \text{(II-3)}$$

where $\sigma = 3.05\text{A}$, $\varepsilon = 54.34\text{K}$, $Q = -0.39 \times 10^{-26}\text{esu}$,[16] and $P_m^1(\cos\theta)$'s are the associated Legendre functions. The variables in the above equation are illustrated in Fig II-1. The separation of the two atoms in each molecule is taken to be a constant, 1.208 A.[16] The dominant part of the potential for O_2 in Eq. II-3 is the atom-atom potential. It is plotted in Fig. II-2 as a function of distance for various orientations. The minimum energy distance depends on the orientations. This potential (Eq. II-3) was first suggested by English and Venables[16] in a general study of diatomic molecular crystals, from which they were able to predict crystal structures with considerable success.

The potential energy of an atom adsorbed on graphite has been put into an analytical form by Steele[19] based on the atom-atom Lennard-Jones potential. Before it is applied here, a derivation of this analytical expression is outlined. Consider the interaction of an adsorbed atom with a perfect two-dimensional lattice having lattice vectors $\vec{a}_1$, $\vec{a}_2$. Let $U_s(\vec{r})$ be the potential energy between the lattice and the adsorbed atom at $\vec{r}$. Due to translational symmetry of the lattice,

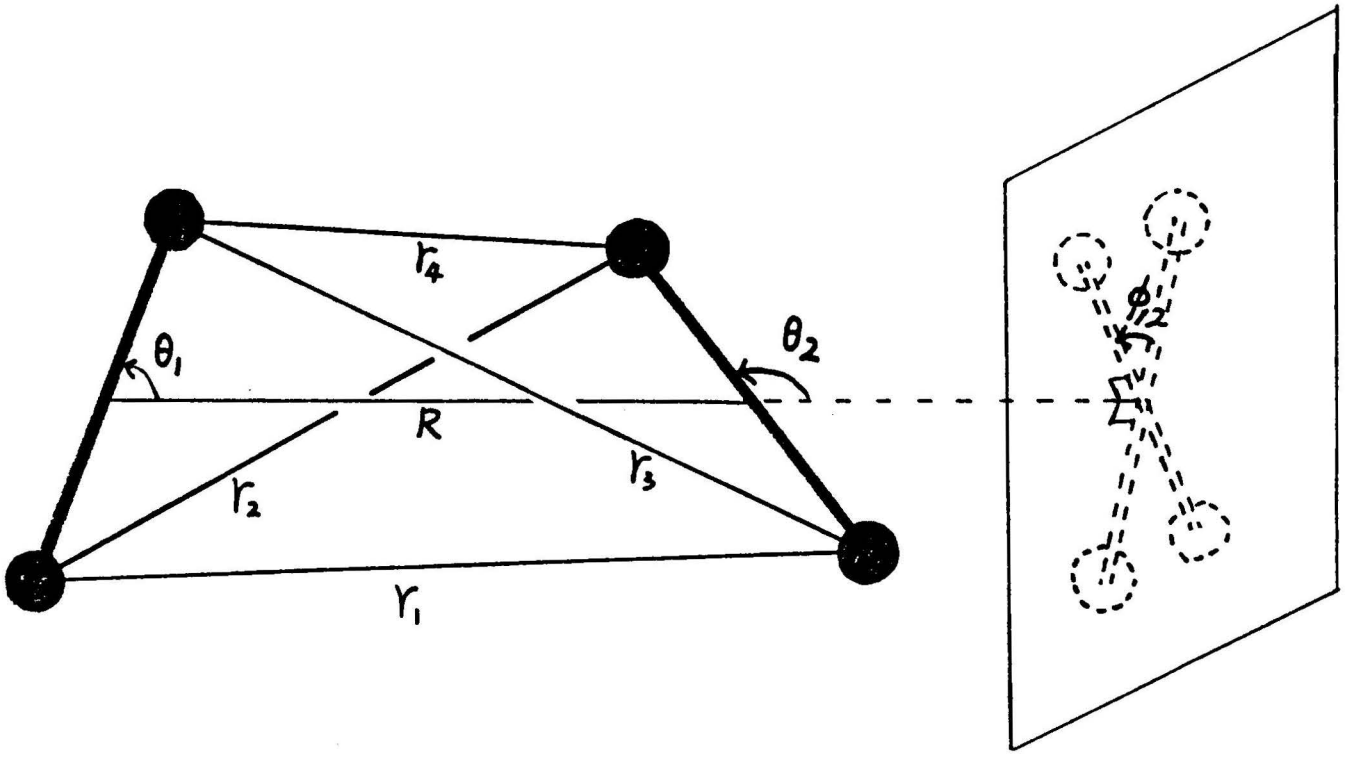

Figure II-1. An illustration for the variables used to determine the potential energy of O_2 pair. The dashed figure is the projection of these two molecules on a plane perpendicular to $\vec{R}$.

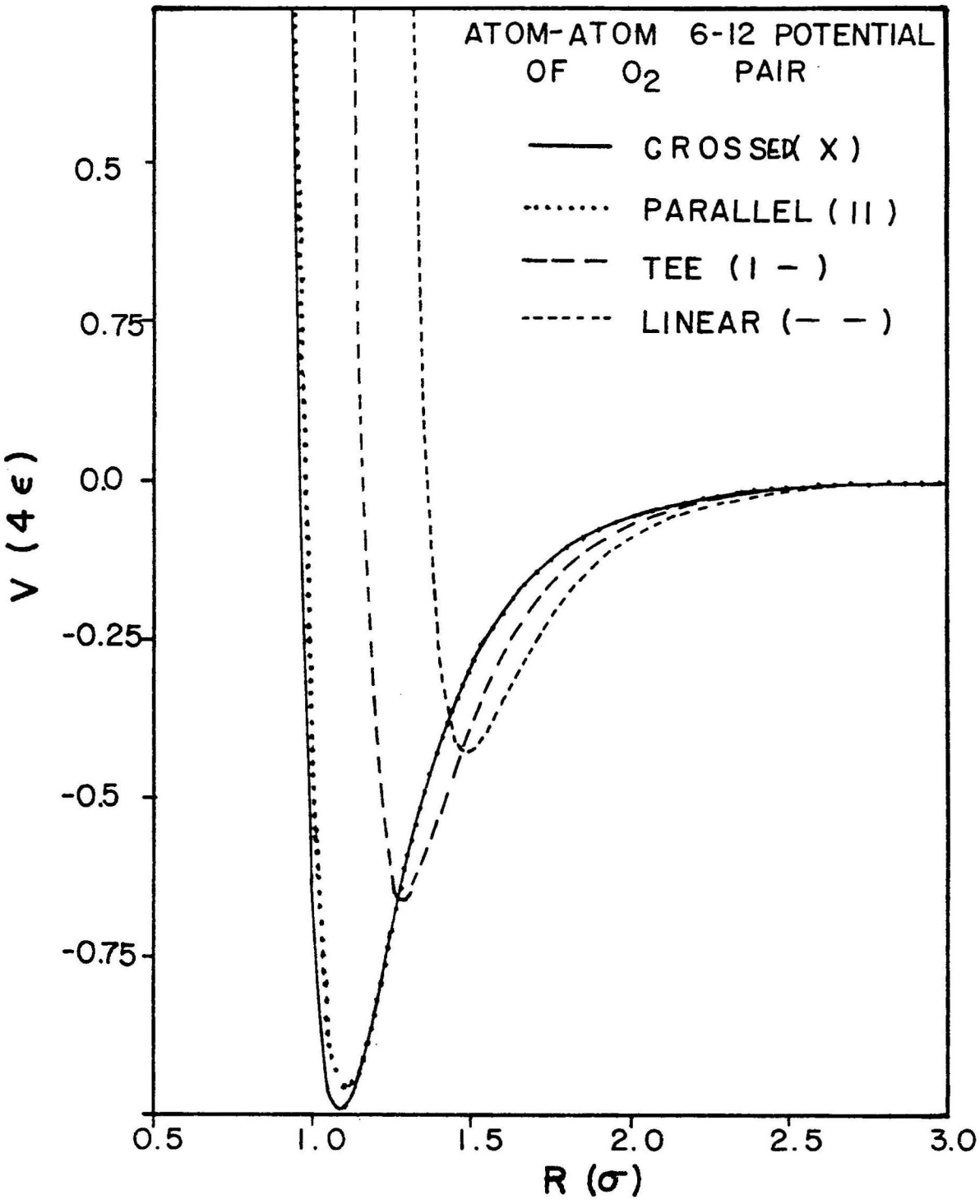

Figure II-2. The atom-atom 6-12 potential for a pair of isolated O_2 molecules with four different orientational configurations versus intermolecular distance.

$$U_s(\vec{r} + l_1\vec{a}_1 + l_2\vec{a}_2) = U_s(\vec{r}) \ , \qquad \text{(II-4)}$$

where l_1 and l_2 are integers. The periodic function $U_s(\vec{r})$ can be represented by a Fourier series,

$$U_s(\vec{r}) = \sum_{\vec{g}} w_{\vec{g}}(z) \exp(i\,\vec{g} \cdot \vec{\tau}) \ , \qquad \text{(II-5)}$$

where z is the perpendicular distance from the adsorbed atom to the lattice, $\vec{\tau}$ is the two-dimensional translation vector with respect to the center of a graphite hexagon, and $\vec{g}$ denotes the reciprocal lattice points, i.e.,

$$\vec{g} = 2\pi[g_1\vec{b}_1 + g_2\vec{b}_2] \ , \qquad \text{(II-6)}$$

where g_1 , g_2 are integers and $\vec{b}_1$, $\vec{b}_2$ are the reciprocal lattice vectors defined by

$$\vec{a}_1 \cdot \vec{b}_1 = \vec{a}_2 \cdot \vec{b}_2 = 1 \ , \qquad \text{(II-7)}$$

and

$$\vec{a}_1 \cdot \vec{b}_2 = \vec{a}_2 \cdot \vec{b}_1 = 0 \ . \qquad \text{(II-8)}$$

With more than one layer in a crystalline solid, the adsorption energy for the adsorbed atom is

$$U_s(\vec{r}) = \sum_{\vec{g}} \sum_{\alpha} w_{\vec{g}}(z_\alpha) \exp(i\,\vec{g} \cdot \vec{\tau}) \ , \qquad \text{(II-9)}$$

where

$$w_{\vec{g}}(z_\alpha) = \frac{1}{a_s} \int_S \exp(-i\,\vec{g} \cdot \vec{\tau})\, U_s(z_\alpha, \vec{\tau})\, d\vec{\tau} \ . \qquad \text{(II-10)}$$

Here $w_{\vec{g}}$ is the Fourier coefficient for the α-th plane located at a distance z_α from the adsorbed atom, S denotes the integration region which is one unit lattice cell, and a_s is the area of the unit cell. If pair-wise additivity is assumed

$$U_s(z_\alpha,\vec{\tau}) = \sum_{l_1,l_2} \sum_k e_{gs}(z_\alpha,\vec{\tau} + l_1\vec{a}_1 + l_2\vec{a}_2 + \vec{m}_k) \ , \qquad \text{(II-11)}$$

where $\vec{m}_k$ is the vector giving the location of k-th atom in a unit lattice cell and e_{gs} is the atom-atom potential between the adsorbed atom and a substrate atom at $-(l_1\vec{a}_1 + l_2\vec{a}_2 + \vec{m}_k)$. Equation II-10 becomes

$$w_{\vec{g}}(z_\alpha) = \frac{1}{a_s} \sum_k \exp(i\,\vec{g}\cdot\vec{m}_k) \int_A \exp(-i\,\vec{g}\cdot\vec{t})\, e_{gs}(z_\alpha,\vec{t})\,d\vec{t} \ , \qquad \text{(II-12)}$$

where A denotes an integration over the entire α-th plane, $\vec{t}$ is the position vector on α-th plane, and $t = |\vec{t}|$ ranges from 0 to infinity.

When $\vec{g} = 0$, Eq. II-12 gives the potential of an atom sitting at a distance z_α above a continuous two-dimensional media with atom density being q/a_s , where q is the number of atoms in a unit cell. If e_{gs} is a function of distance, $\rho = (z_\alpha^2 + t^2)^{\frac{1}{2}}$, only, then Eq. II-12 can be simplified,

$$w_{\vec{g}}(z_\alpha) = \frac{2\pi}{a_s} \sum_k \exp(i\,\vec{g}\cdot\vec{m}_k) \int_o^\infty J_o(gt)\, e_{gs}(\rho)\, t\,dt, \qquad \text{(II-13)}$$

where J_o is the Bessel function. With the Lennard-Jones potential the remaining integral is readily done since

$$\int_o^\infty J_o(gt) \left(\frac{1}{z^2 + t^2}\right)^{n+1} t\,dt = \frac{1}{n!}\left(\frac{g}{2z}\right)^n K_n(gz) \ , \qquad \text{(II-14)}$$

where K_n is the modified Bessel function of the second kind. For the 12-6 potential with parameters ε_{gs} and σ_{gs}, we obtain

$$\frac{U_s(\vec{r})}{\varepsilon_{gs}} = \frac{2\pi}{a_s} \sum_{\alpha} \left[q\left(\frac{2}{5}\frac{\sigma_{gs}^{12}}{z_\alpha^{10}} - \frac{\sigma_{gs}^{6}}{z_\alpha^{4}}\right) + \sum_{\vec{g}\neq 0} \sum_{k=1}^{q} \exp(i\,\vec{g}\cdot[\vec{m}_k + \vec{\tau}]) \right.$$
$$\left. \times \left(\frac{\sigma_{gs}^{12}}{30} \left(\frac{g}{2z_\alpha}\right)^5 K_5(gz_\alpha) - 2\sigma_{gs}^{6} \left(\frac{g}{2z_\alpha}\right)^2 K_2(gz_\alpha) \right) \right] \qquad \text{(II-15)}$$

So far, all the equations have been derived exactly. In the following, several approximations will be employed. First of all, since $K_n(x)$ decays quite rapidly with x, only the surface layer makes significant contribution to the $\vec{\tau}$ dependent part of Eq II-15. Secondly, at $z \approx \sigma_{gs}$, only the smallest g's contribute. Equation II-15 can then be written for the graphite as

$$\frac{U_s(\vec{r})}{\varepsilon_{gs}} = E_o + E_1\left(\cos\,(\vec{G}_1\cdot\vec{\tau}) + \cos\,(\vec{G}_2\cdot\vec{\tau}) + \cos\,[(\vec{G}_1+\vec{G}_2)\cdot\vec{\tau}]\right), \qquad \text{(II-16)}$$

where

$$E_o = \frac{4\pi}{a_s} \sum_{\alpha} \left(\frac{2}{5}\frac{1}{z^{10}} - \frac{1}{z^{4}}\right), \qquad \text{(II-17)}$$

$$E_1 = -\frac{4\pi}{a_s}\left[\frac{1}{30}\left(\frac{G}{2z}\right)^5 K_5(Gz) - 2\left(\frac{G}{2z}\right)^2 K_2(Gz)\right], \qquad \text{(II-18)}$$

and $\vec{\tau}$ is relative to the center of a graphite surface hexagon. Here, the lengths are in units of σ_{gs}, energies are in ε_{gs}, and

$$G = |G_1| = |G_2| = 2\pi/(a_1\cos 30^o). \qquad \text{(II-19)}$$

The quantities a_1 [19], $\vec{G}_1$ and $\vec{G}_2$ are illustrated in Fig. II-3.

One more approximation is taken to reduce the number of terms for E_o in Eq. II-17. Since the z^{-10} term diminishes rapidly, only the first layer contribution is kept. The summation of z^{-4} for $\alpha > 1$ is replaced by the integrated value. Thus,

$$E_o = \frac{4\pi}{a_s}\left[\frac{2}{5z^{10}} - \frac{1}{z^4} - \frac{1}{3\Delta z(z + 0.61\ \Delta z)^3}\right], \qquad \text{(II-20)}$$

where Δz is the separation between graphite layers, and the integration from $z = 0.61\ \Delta z$ is found to give a more accurate representation to the layer summation than $z + \Delta z$. Δz here has the value 3.35 Å.[20]

For the absorption energy of oxygen molecules on graphite in this work, two further approximations are considered. If the atom-atom interaction is again assumed, then

$$V_2 = \sum_{\text{molecules}} U_s(z_1, \vec{\tau}_1) + u_s(z_2, \vec{\tau}_2) \quad , \qquad \text{(II-21)}$$

where z_1 , $\vec{\tau}_1$ and z_2 , $\vec{\tau}_2$ are the locations of the two atoms of a molecule respectively. The Lennard-Jones parameters are $\varepsilon_{gs} = \sqrt{\varepsilon \times \varepsilon_{c-c}}$ and $\sigma_{gs} = 0.5(\sigma + \sigma_{c-c})$ with $\varepsilon_{c-c} = 28K$ and $\sigma_{c-c} = 3.4$ Å .[20] Precisely this form of potential has been used by Steele[20] in the study of adsorbed nitrogen films. His results compared favorably with the experimental phase diagram and the heat of adsorption. Fuselier *et al.* [21] predicted the orientational configuration of these nitrogen films with this potential, too. Their results were consistent with experiments.[22] If, however, the isotropic potential for the oxygen molecule represents the adsorption energy better, then

$$V_2 = \sum_{\text{molecules}} U_s(z, \vec{\tau}) \qquad \text{(II-22)}$$

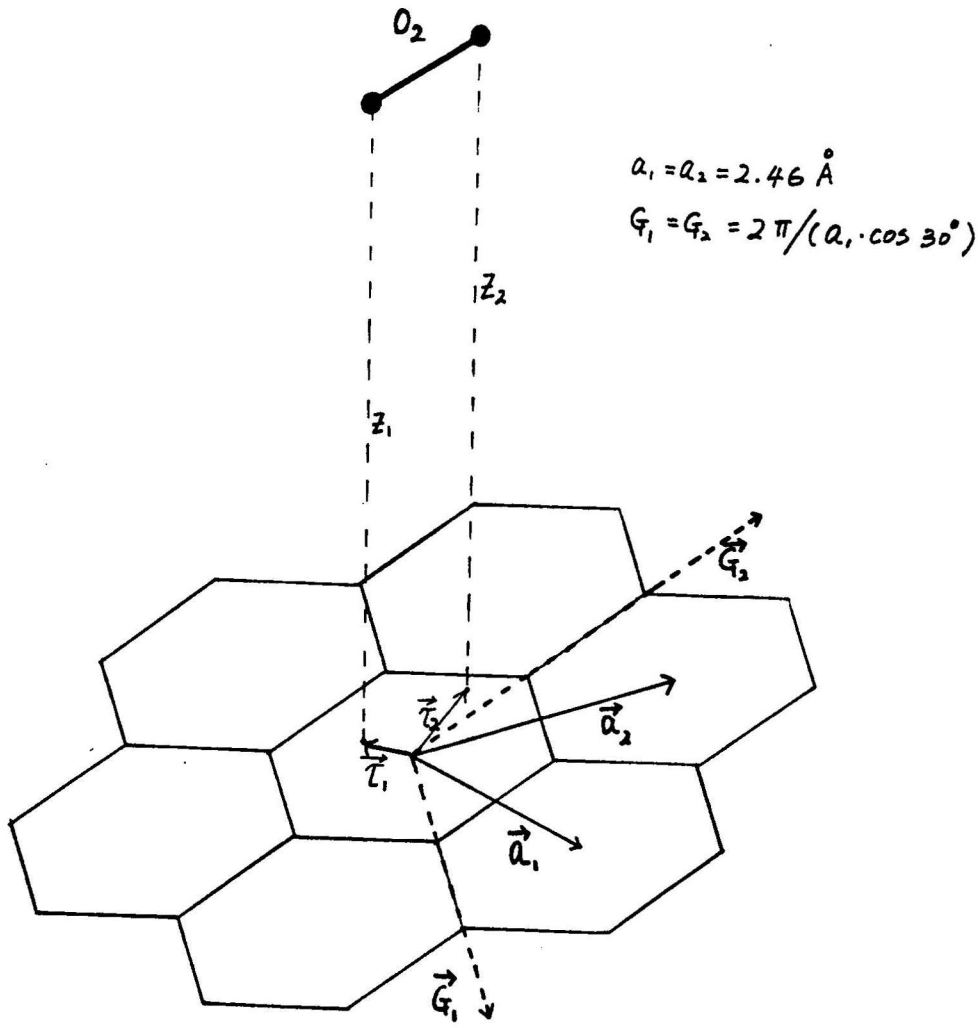

Figure II-3. The schematic illustration for an adsorbed oxygen molecule on the graphite basal plane.

where z and $\vec{\tau}$ are the coordinates for the molecular center. The Lennard-Jones parameters are $\sigma_{gs} = 1/2(\sigma_{O_2-O_2} + \sigma_{c-c})$ and $\varepsilon_{gs} = (\varepsilon_{O_2-O_2} \times \varepsilon_{c-c})^{\frac{1}{2}}$, where $\sigma_{O_2-O_2} = 3.431$ Å and $\varepsilon_{O_2-O_2} = 110.9$ K.[23]

CHAPTER III

METHODS

Section III-A, Monte-Carlo Method

The expectation value of a thermodynamic variable A at temperature T is given by the emsemble average,

$$\langle A \rangle = \int d\tau\ A(\tau)\ P(\tau) / \int d\tau\ P(\tau)\ , \qquad \text{(III-1)}$$

where $P(\tau)d\tau$ is the probability of finding the system in a phase space element $d\tau$. In this work, it is assumed that $P(\tau)$ follows the Maxwell-Boltzman distribution, that is

$$P(\tau) \propto \exp\ (-E/kT)\ ,$$

where E is the total potential energy of the system and k is the Boltzman constant.

For a system with N oxygen molecules adsorbed on the graphite, $5N$ degrees of freedom are involved. Three specify the center of mass position and two specify the orientation of each molecule. The $5N$ variable integration is carried out using Monte-Carlo method. A standard Monte-Carlo calculation[24] would generate points randomly and weight them by $P(\tau)$, i.e.,

$$\langle A \rangle \tilde{=} \overline{A} = \sum_{i=1}^{n} A(\xi_i)\ P(\xi_i) / \sum_{i=1}^{n} P(\xi_i)\ , \qquad \text{(III-2)}$$

where n is the number of samples. This method is not practical because of the infinite range of phase space and the localized strength of $\exp(-E/kT)$. A modified Monte-Carlo method is employed

where the sample configurations are chosen according to the probability P and weighted equally, i.e.,

$$\overline{A} = \frac{1}{n} \sum_{i=1}^{n} A(\xi_i) \ . \qquad \text{(III-3)}$$

In their study of the equation of state of a two-dimensional system of hard disks, Metropolis *et al.*[25] invented a way to choose these points with a biased random walk Markov Chain of n steps. In each step $P(\tau_{i+1})/P(\tau_i)$ for two consecutive configuration is calculated and used to determine whether the new configuration is to be accepted. This method has been applied to isolated clusters of spherical molecules.[26] The same procedure is used here for the adsorbed oxygen clusters with additional degrees of freedom for molecular orientations. Instead of specifying molecular orientation by two angular variables, three variables are used giving the direction cosines of each molecular axis, because it is computationally much easier to sample three Cartesion coordinates than two angular coordinates.

Initially, the N molecules are arbitrarily positioned and oriented at $(\vec{r}_1 , \vec{\omega}_1 , \vec{r}_2 , \vec{\omega}_2 , \text{----- } \vec{r}_N , \vec{\omega}_N)$, where $\vec{r}_i$ is the position vector for the center of mass of molecule i and $\vec{\omega}_i$ is the unit vector specifying the orientation of molecule i . The energy E and the probability $\exp(-E/kT)$ are calculated for this configuration. A randomly chosen molecule is then allowed to move randomly to a new location. This specifies a trial configuration for which the energy and probability are calculated. According to a set of criteria related to the probability of the trial configuration and the previous configuration, the trail configuration is either accepted or rejected.[25] If accepted, the value A of this configuration is

incorporated into the sum (Eq. III-3). If rejected, the configuration is returned to its original point, the value A of the original configuration is added to the sum. The procedure is repeated next by changing the orientation instead of the position. The direction vector of a randomly chosen molecule is allowed to move randomly and then normalized to a unit vector. The same criteria are used to judge the acceptance of this trial configuration. The value for the appropriate configuration is added to the sum. The above procedure continues by alternately moving locations and orientations until all n configurations have been chosen.

To avoid "initial transient," which are drastic changes in system properties in the beginning of the random walk, the first approximately 80,000 configurations are not included in the averaging process. Up to 800,000 configurations are computed per run and divided into bins of 2000 configurations each to examine the convergence of average energy. The maximum allowed displacement of a molecule from one configuration to the next one (the step size) is adjusted at the end of each bin so that the rate of acceptance is about 50%. The step size for the direction cosines is adjusted in a similar manner. However, its upper limit is set at 0.2, regardless how high the rate of acceptance for orientational move might be.

Section III-B, Energy Minimization

The equilibrium lattice configuration of an infinite monolayer oxygen films adsorbed on graphite is determined by minimizing the total energy of the system using "Pattern Search."[27] As an example, we describe the pattern search for a two variable case, as shown in Fig. II-1.

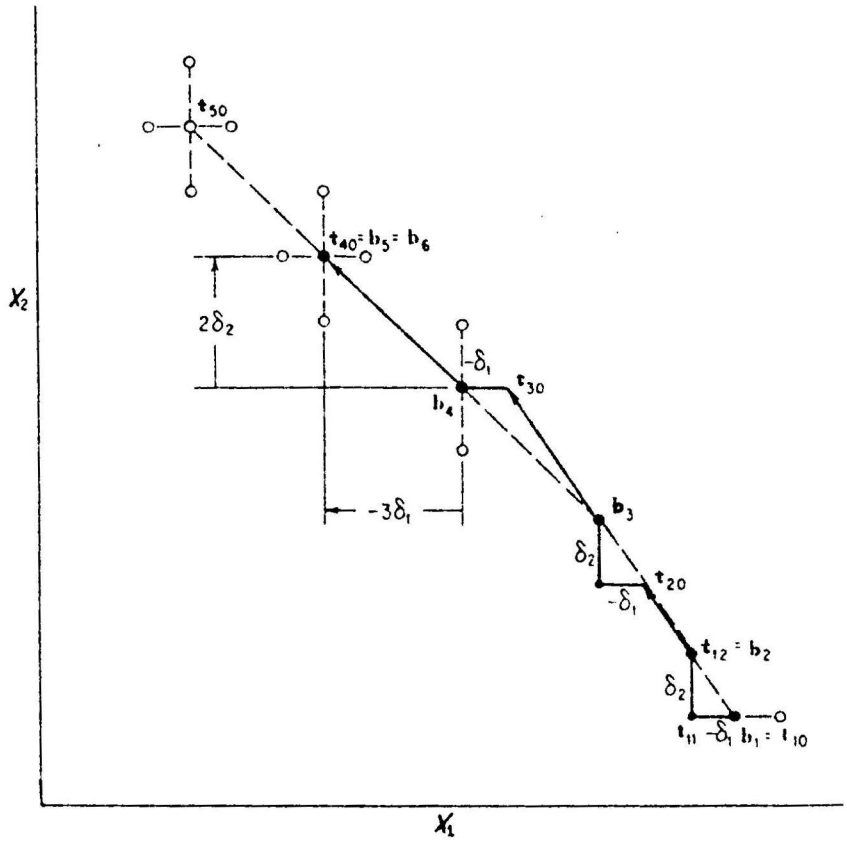

Figure III-1. Looking for a minimum point of a two variable function by Pattern Search.

An initial point $\vec{b}_1 = (x_i, y_i)$ is chosen and an exploration is started from this point with given step sizes δ_1 and δ_2. We search along the x direction first to find a point $\vec{t}_{11}$ as the following:

$$\vec{t}_{11} = \begin{cases} (x_i + \delta_1, y_i) & \text{if } f(x_i + \delta_1, y_i) < f(x_i, y_i) \\ (x_i - \delta_1, y_i) & \text{if } f(x_i - \delta_1, y_i) < f(x_i, y_i) \leq f(x_i + \delta_1, y_i) \\ \vec{b}_1 = (x_i, y_i) & \text{if none of above.} \end{cases} \qquad \text{(III-4)}$$

Then a search along the y direction from $\vec{t}_{11}$ is made in a similar manner with δ_2 instead of δ_1 to get $\vec{t}_{12}$. Let us assign $\vec{b}_2 = \vec{t}_{12}$. Now we have moved from $\vec{b}_1$ to $\vec{b}_2$ and a pattern is established, next we follow this pattern by doubling the first move to get $\vec{t}_{20}$, i.e.,

$$\vec{t}_{20} = \vec{b}_1 + 2(\vec{b}_2 - \vec{b}_1) = 2\vec{b}_2 - \vec{b}_1 . \qquad \text{(III-5)}$$

Then a local exploration around $\vec{t}_{20}$ is carried just like that around $\vec{b}_1$ to locate b_3. Thus, $\vec{b}_4$, $\vec{b}_5$ --- $\vec{b}_i$ will be similarly determined, each being positions of lower energy until the point $\vec{b}_{i+1}$ is reached, which does not have lower energy than $\vec{b}_i$. Then the pattern is destroyed and a new pattern is established by starting at $\vec{b}_i$, just as was done around $\vec{b}_1$. If no better point can be found around $\vec{b}_i$, the step sizes are reduced to half their previous values and the search is continued. This process is carried on until a new reduced step size is less than the originally specified minimum.

A two-sublattice structure is assumed for the absorbed film. The molecules of the first sublattice are located at the rectangular

sublattice points and the molecules of the other sublattice are located at the centers of the super lattice rectangles. Thus, there are 6 degrees of freedom for the film at a given density. One is for the lattice constant along one direction of the lattice rectangle, a second is for the height of the film above ths substrate, and there are two for the molecular orientation on each sublattice. For calculational convenience, the three direction cosines are used to specify the molecular orientation on each substrate. Therefore, eight independent variables are used in our minimization method, but the normalized direction cosines are used to determine potential energy.

CHAPTER IV

RESULTS

In this chapter, the results of our study on O_2 clusters and films adsorbed on graphite are presented. The structures, orientations, registry to substrate, orientational order-disorder transitions, melting and dissociations of two-dimensional clusters are discussed in section IV-A and IV-B. In section IV-A, the interaction of the oxygen molecules with the graphite surface is neglected. In section IV-B, an atom-atom potential is used for the oxygen-graphite interaction. The energies, orientations, and structures of infinite films are described in section IV-C. Energies are in units of $4\epsilon = 217.34$ K and lengths are in units of $\sigma = 3.05$ A , unless otherwise mentioned. The surface plane is defined to be the x-y plane. The z-direction is normal to and away from the substrate. The origin of the coordinate system is fixed at the center of a graphite hexagon on the surface layer.

Section IV-A, Two-dimensional Oxygen Clusters Without Surface Interaction

This work assumes that the graphite surface only exerts a uniform background force to maintain the oxygen molecules centers on the x-y plane, which is parallel to the substrate surface. This approximation is equivalent to assuming an isotropic oxygen-graphite interaction (Eq. II-23), which acts to keep the O_2 molecular centers at the same distance from the substrate but exerts no orientational force. Cluster sizes with $2 \leq N \leq 12$ are studied by the Monte-Carlo method.

At low temperatures, the O_2 molecules in clusters with $N \geq 2$ are perpendicular to the substrate plane and parallel to each other. They librate about their equilibrium orientations. Due to the analogy in structure with β-films, the clusters studied in this section are named β-clusters. Because of the symmetry of the O_2 molecule, there are two degenerate orientation states separated by π for each molecule. Thus the thermal average of a molecular direction cosine along $\hat{z}$, $< \gamma >$, is either near 1 or -1. The energy states are identical, but the barrier between them prevents the molecule flipping from one state to the other at low temperature. However, as the temperature increases, the libration of the molecules increases and the probability that these molecules can overcome the barrier increases. At some temperature $T_{OD}(N)$, these two orientational degenerate states become mixed as the molecules undergo hindered rotation, signaling the onset of an orientational order-disorder phase transition. The hindered rotors have orientational probabilities peaked at $\gamma = \pm 1$. With increasing temperature, the orientational distribution smears out and the molecules approach free rotors.

The average bond length between the molecules and the bond length fluctuation in the crystallite state increase with rising temperature, until the temperature reaches $T_M(N)$. At this temperature, the cluster starts to lose its well-defined structures. Evidence to be presented later in this section indicates that this is a structural order-disorder transition analogous to the melting phenomenon in bulk systems. Therefore, $T_M(N)$ is assigned as the melting temperature for the cluster with size N.

For temperatures $T > T_M$, the clusters are fluid like until $T_B(N)$, where the cluster dissociates. This transition is identified when the average energy of each bin in the Monte-Carlo process increases montonically and the binding energy approaches zero. A detailed discussion on identifying the melting and the dissociation transitions have been given by Etters and Kaelberer[26] for three-dimensional rare gas clusters. Similar arguments apply to this work. A brief discussion will be presented in the subsection describing these transitions.

Section IV-A-1, Structures

The $N = 2$ dimer has an "X" configuration, i.e., the two molecular axes and the bond connecting the centers of the two molecules are mutually perpendicular. The structures for $N \geq 3$ have a common feature. All of the molecular axes are perpendicular to the surface plane. In Fig. IV-1, the configurations are illustrated, each circle represents the center of a molecule. Shapes are determined by the expectation values of the O_2 positions, which are at points of maximum coordination number. The equilibrium configurations for $N < 6$ are uniquely specified. Isomeric states first appear for $N = 6$ and its ground state forms an incomplete hexagon. The other two isomers, also shown in Fig. IV-1, have energies very close to the ground state. $N = 7$ forms a hexagon and $N = 12$ is formed from three interpenetrating hexagons.

Section IV-A-2, Orientational Order-disorder Phase Transitions

Orientational order-disorder phase transition are found for all clusters with $N \geq 3$. Using $N = 3$ as a prototype, there are the

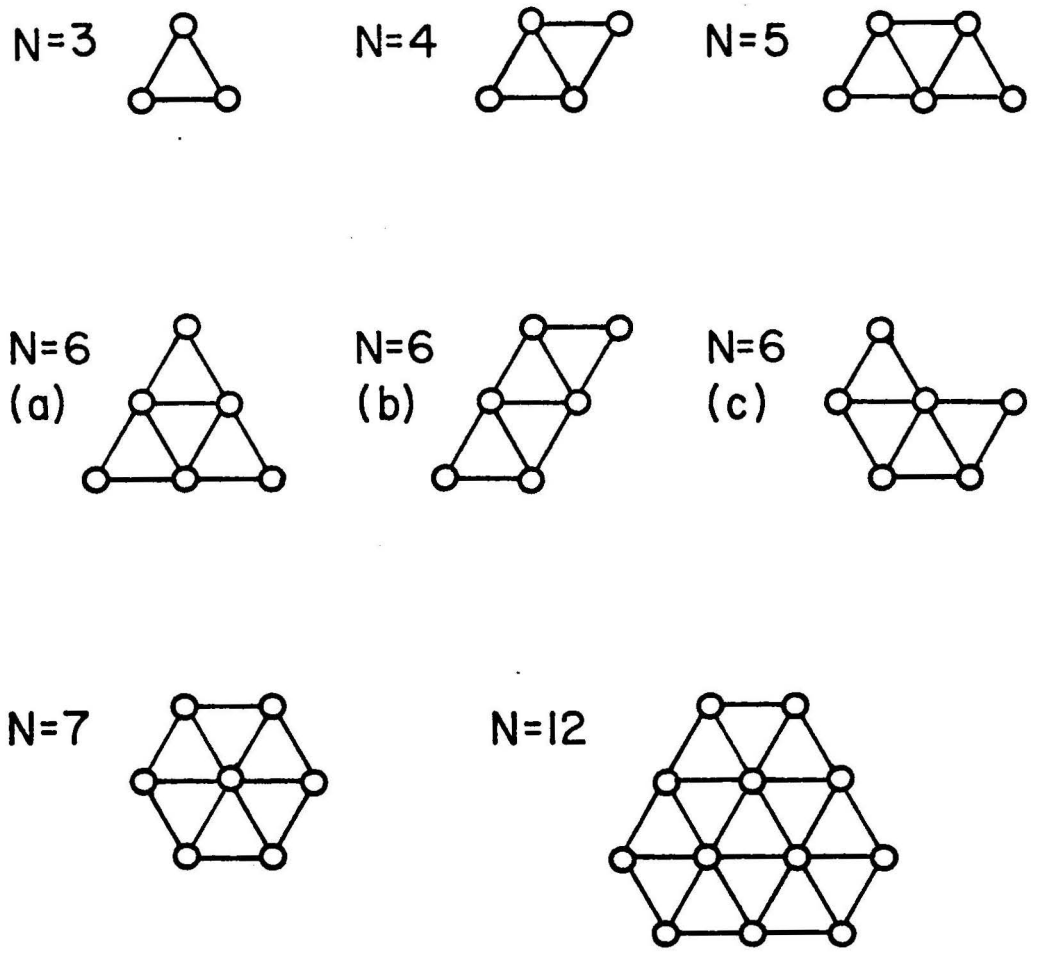

Figure IV-1. The structures of two-dimensional clusters without surface interaction (β-clusters). The molecular axes are perpendicular to the cluster plane. The molecular centers are symbolized by "o".

following physical evidences for this transition. The direction cosine of each molecular axis along the $\hat{z}$ direction, γ, begins to fluctuate between positive and negative numbers at 4.5 K. Figure IV-2 is presented to show how the thermal average of $\cos \theta_{ij}$, i,j = 1,2,3, varies with temperature. For $T < 4.5$ K, these values are close to 1 but decrease slowly with increasing temperature due to increasing librations. Above $T = 4.5$ K, they drop substantially and are much smaller than the thermal average of $|\cos \theta_{ij}|$, i.e., $\langle|\cos \theta_{ij}|\rangle$ (see Fig. IV-3). This indicates that the molecules are reversing their orientations but they are not totally free rotors. A plot of $\langle\gamma\rangle$ versus temperature (not shown) gives similar information as Fig. IV-2. The average of $\langle|\cos \theta_{ij}|\rangle$, i, j = 1,2,3, is plotted in Fig. IV-3 as a function of temperature. The data points follow a straight line for $T < 5.5$ K and another line for $T > 5.5$ K with different slope. This indicates a property change at $T = 5.5$ K. The energy per molecule versus temperature curve (Fig. IV-4) also has a sudden change in its slope at $T \approx 5$ K. By all the means discussed above, we conclude that an orientational order-disorder phase transition takes place at $T \approx 5$ K.

For clusters with $N \geq 4$, not all the molecules are equally bound. For example, in the $N = 4$ cluster, the two molecules with three nearest neighbors are more tightly bound than the other two which have only two nearest neighbors. As the temperature increases, the two less tightly bound molecules become disordered first, while the other two remain orientationally ordered until a higher temperature, where they also become disordered. The notation $T_{ODk}(N)$ is used for the orientational order-disorder transition temperature for the

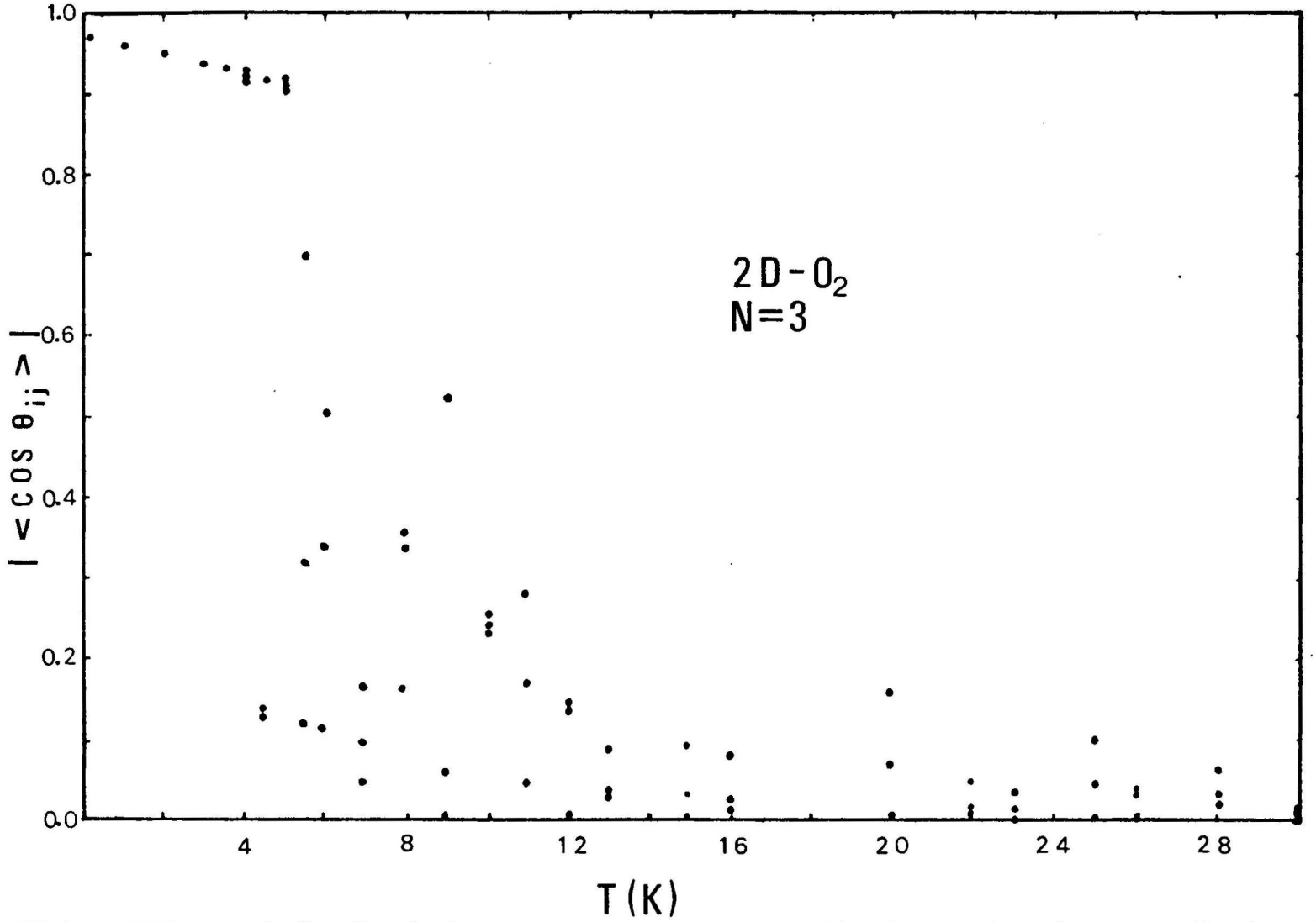

Figure IV-2. $\langle COS\theta_{ij} \rangle$ of N = 3 β-cluster versus temperature. The three pair values are all plotted unless they are so close that they cannot be distinguished with the resolution of this graph.

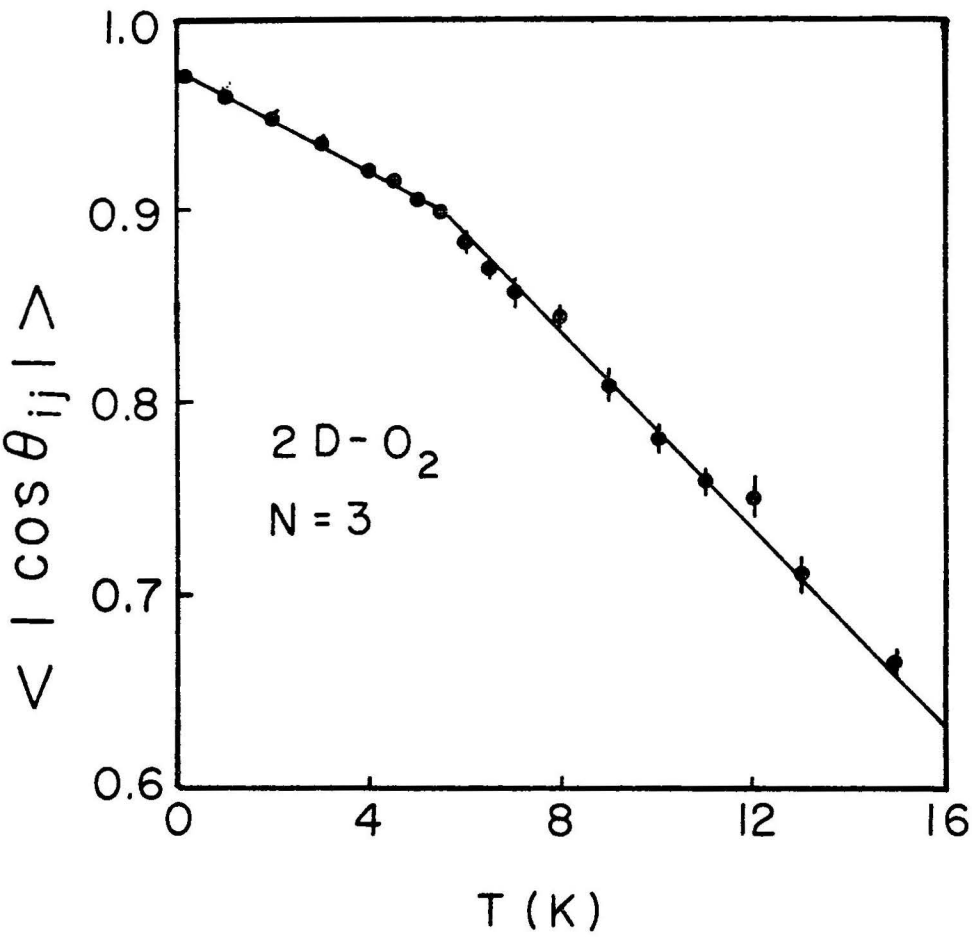

Figure IV-3. $\langle|\cos\theta_{ij}|\rangle$ versus temperature for N = 3 β-cluster. Average of the three pair values are plotted, the error bars indicate the spreadings of these three values.

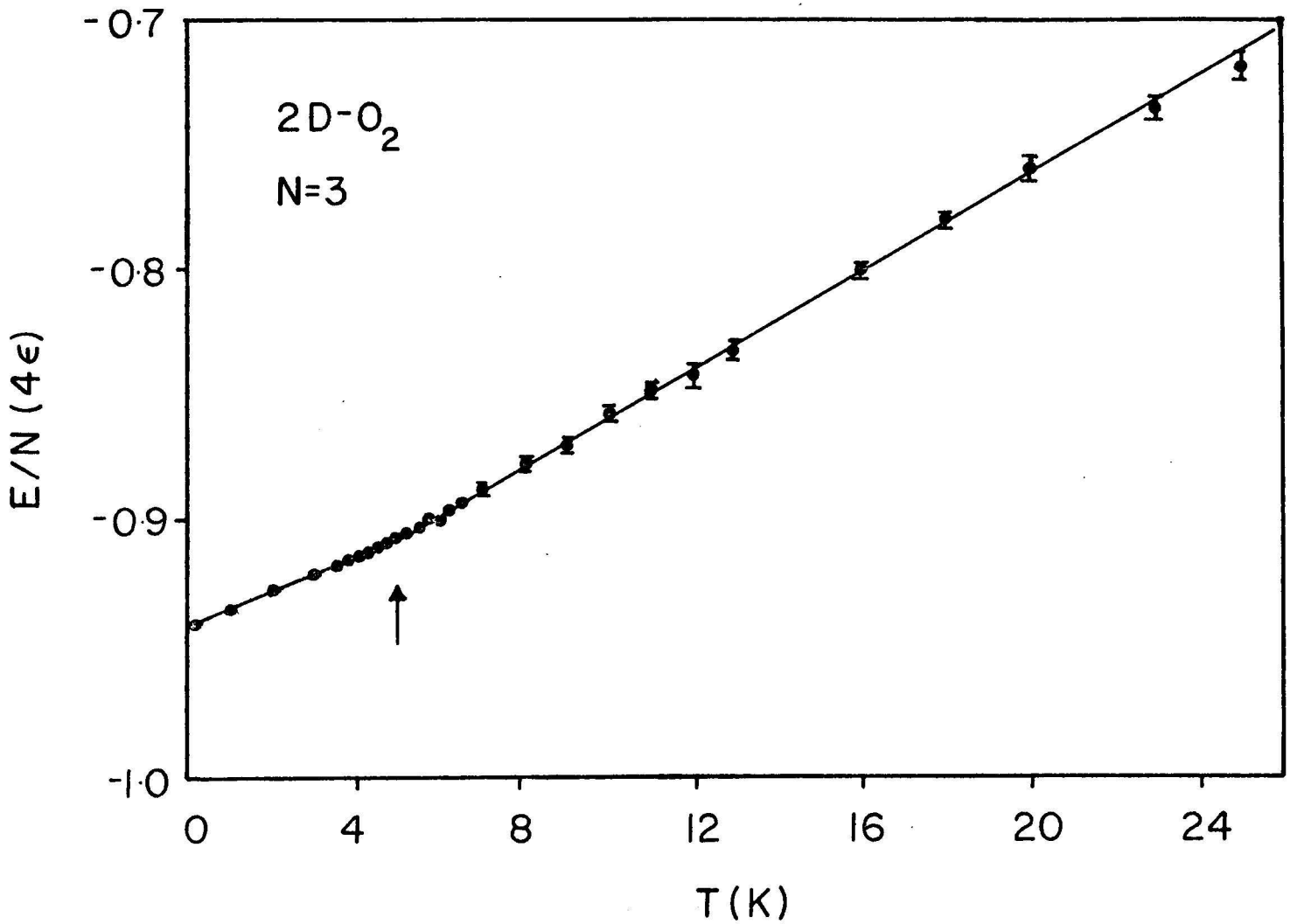

Figure IV-4. Energy per molecule versus temperature for N = 3 β-cluster. Arrow marks the place for orientational order-disorder transition.

molecules with k nearest neighbors in clusters having N molecules. The energy versus temperature curves and the $\langle|\cos\theta_{ij}|\rangle$ versus temperature curves for $N = 4,5,6,7,$ and 12 are plotted in Figs. IV-5 to IV-14. T_{OD2} and T_{OD3} are clearly shown in these figures. However, T_{OD4} for $N = 5$, $N = 6$ equilateral triangle, and $N = 12$ can be detected only by the $\langle\gamma\rangle$'s of the corresponding molecules. This is probably because this transition is very close to the melting point. The interference of property changes due to both transitions make it hard to identify T_{OD4}. The center molecule in the $N = 6$ incomplete hexagon is not orientationally disordered until melting occurs. Neither are the center molecules for $N = 7$ and $N = 12$. All of the T_{OD}'s and their uncertainties are listed in Table IV-1.

As an additional piece of collaborating evidence, it is found that the intermolecular bond lengths change with temperature at different rates in the different orientational phases. That is, the expansion coefficients are different in different phases. In Fig. IV-15, the average nearest neighbor distances versus temperature curves in crystallite phase region are plotted. All except those associated with T_{OD4} can be detected by an abrupt change in slope.

At $T > T_{OD}$, the rotation gradually approaches free rotor states. However, even near T_M, the melting temperature, the molecules are not completely free rotors as evidenced by $\langle|\cos\theta_{ij}|\rangle$ values. For free rotors, $\langle|\cos\theta_{ij}|\rangle$ would be 0.5, but our data are still higher than this.

Section IV-A-3, Melting Transitions

As the temperature increases, the fluctuations of molecular positions about equilibrium increase until melting at $T = T_M$, where

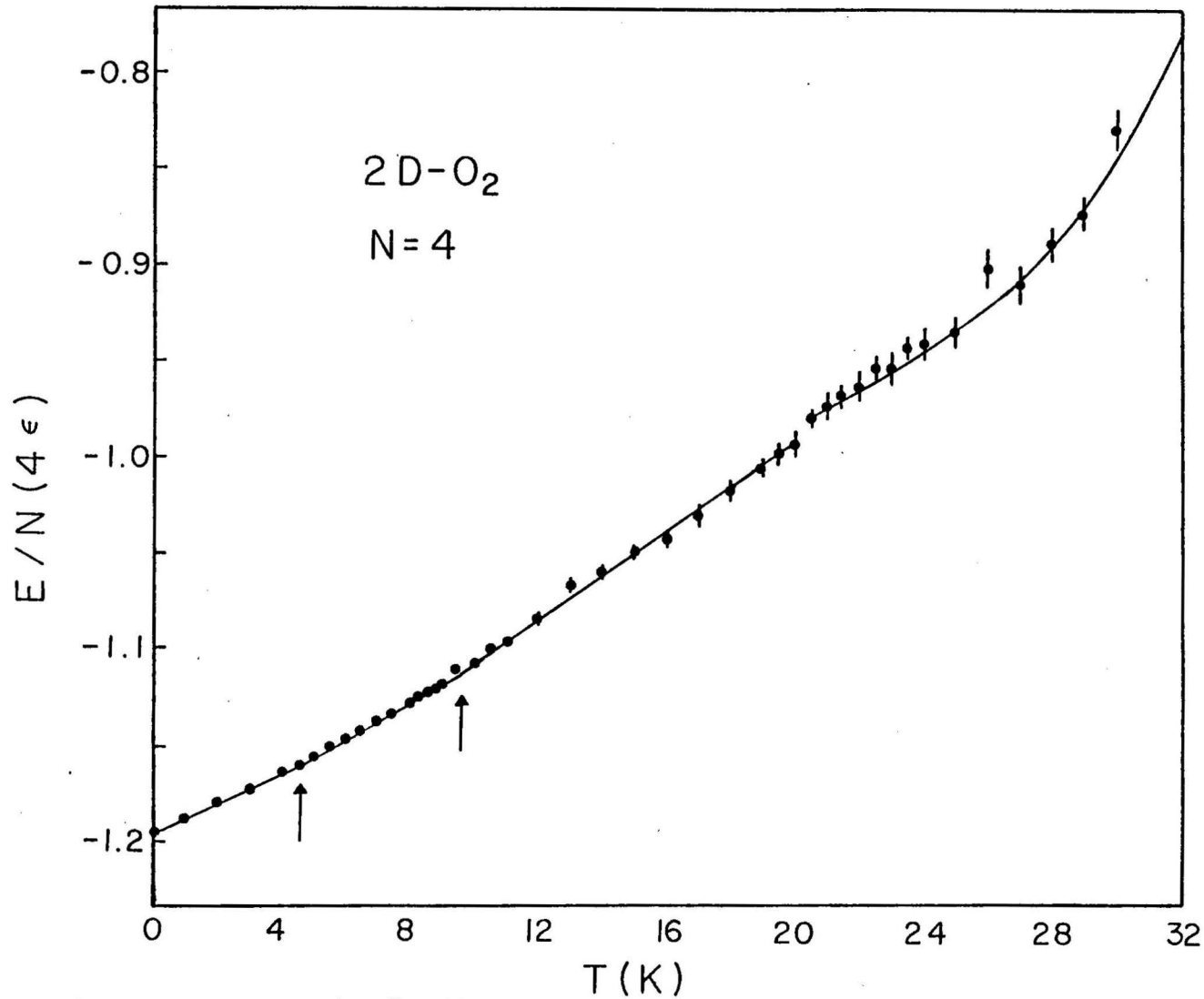

Figure IV-5. Energy per molecule for N = 4 β-clusters. Arrows mark the places for orientational order-disorder transitions.

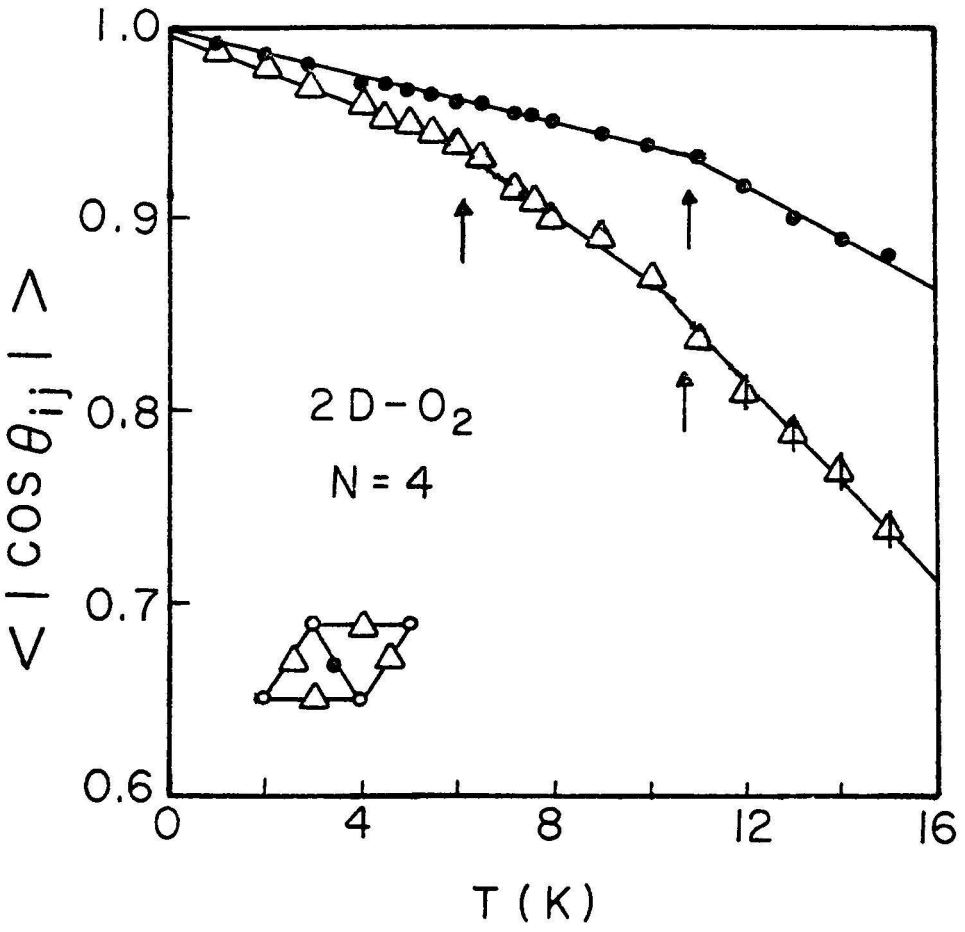

Figure IV-6. $\langle|\cos\theta_{ij}|\rangle$ for N = 4 β-cluster. The value for the pair marked by "•" in insert is plotted with "•". The average value for the 4 pairs marked by "Δ" is plotted with "Δ", error bar indicates the spreading of these 4 pair values.

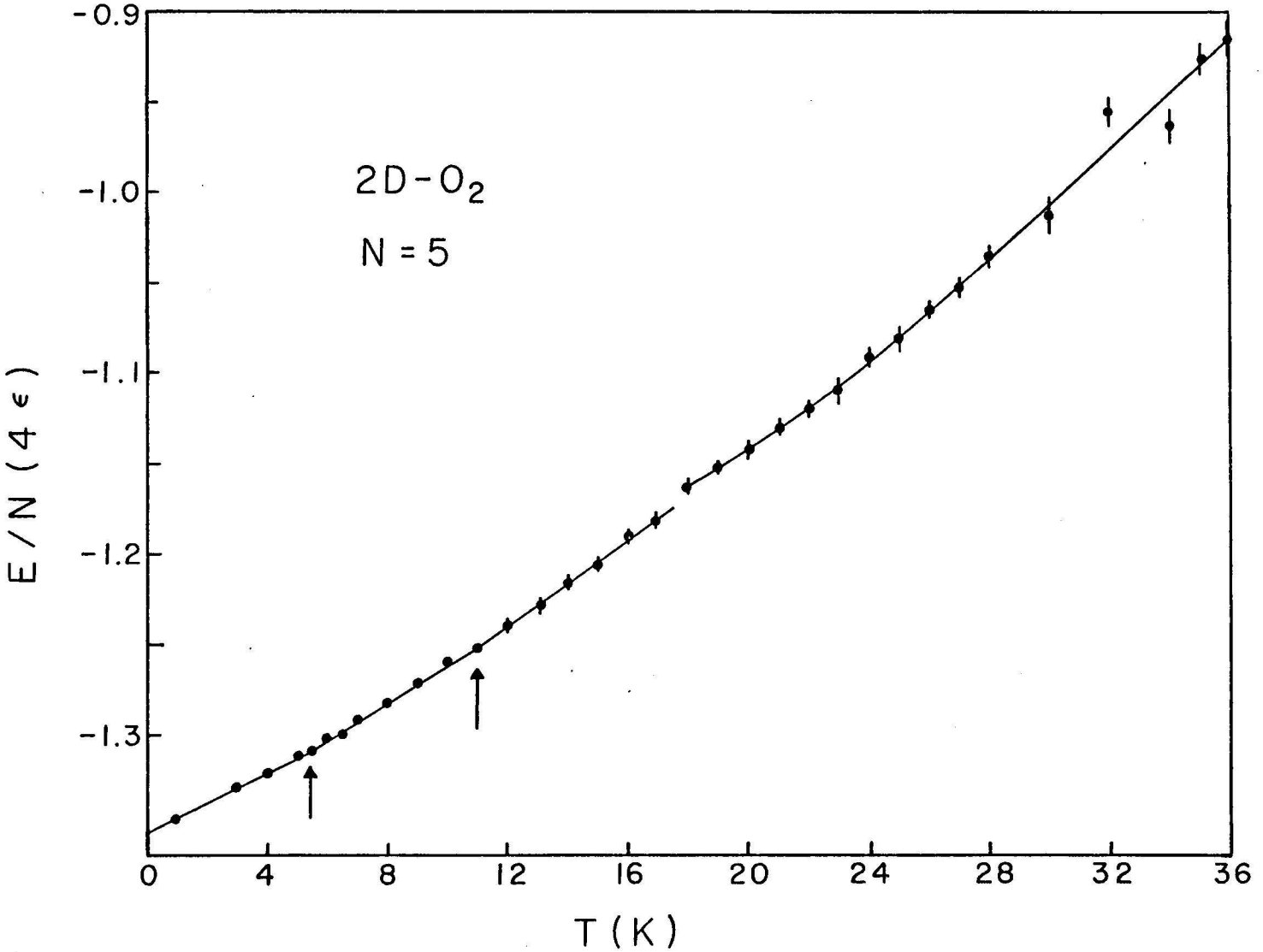

Figure I7-7. Energy per molecule for N = 5 β-cluster. Arrows mark the places for orientational order-disorder transitions.

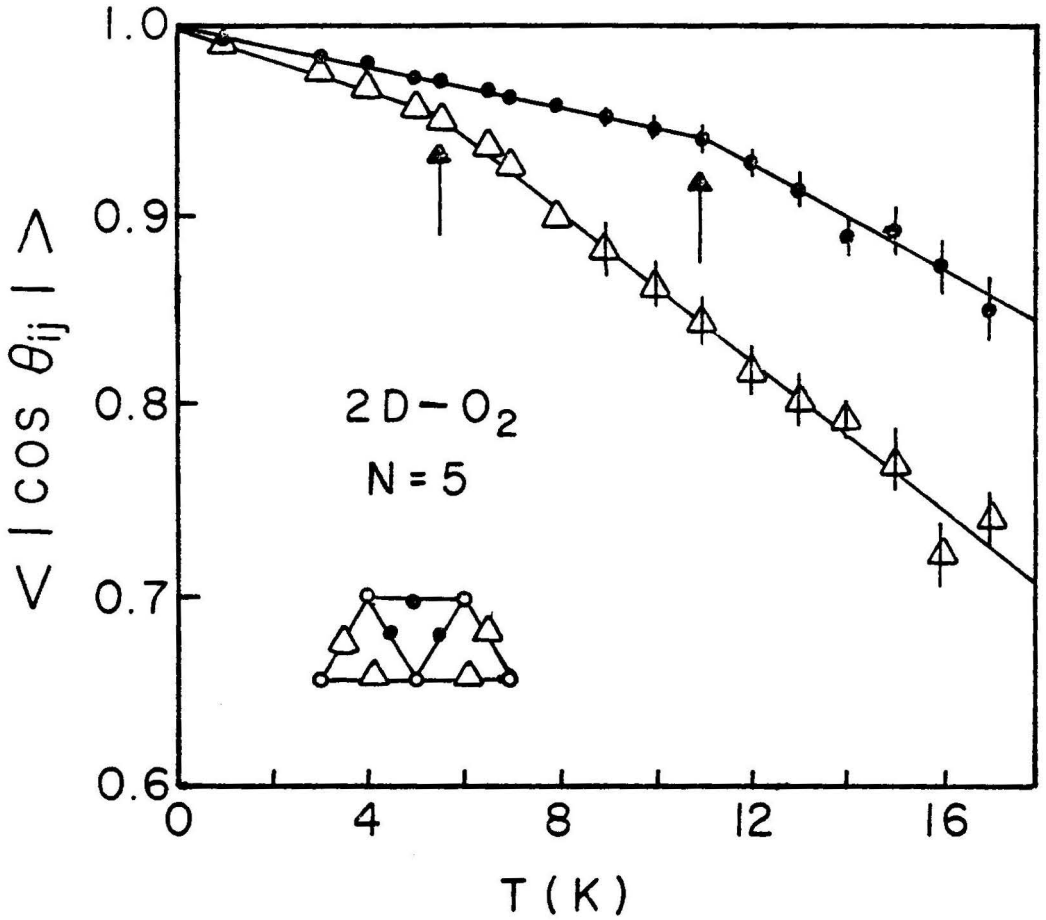

Figure IV-8. $\langle|\cos\theta_{ij}|\rangle$ for N = 5 β-cluster. "•" and "Δ" in curves show the average values for the pairs marked with same signs in insert, respectively. Error bar indicates the spreading of associated pair values.

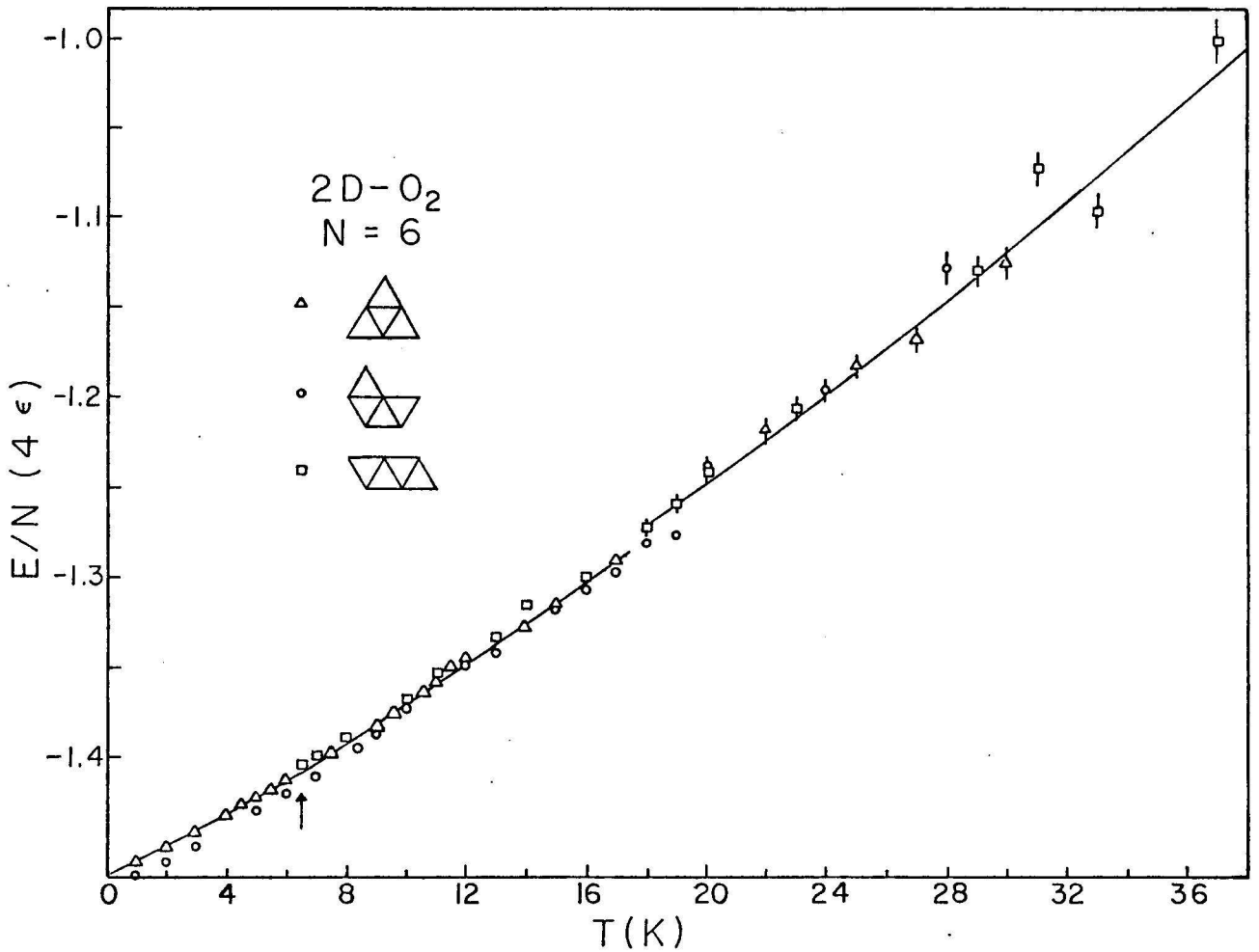

Figure IV-9. Energy per molecule for the three isomeric states of N = 6 β-cluster. The solid curve at T < 18 K is drawn by fitting "Δ"'s.

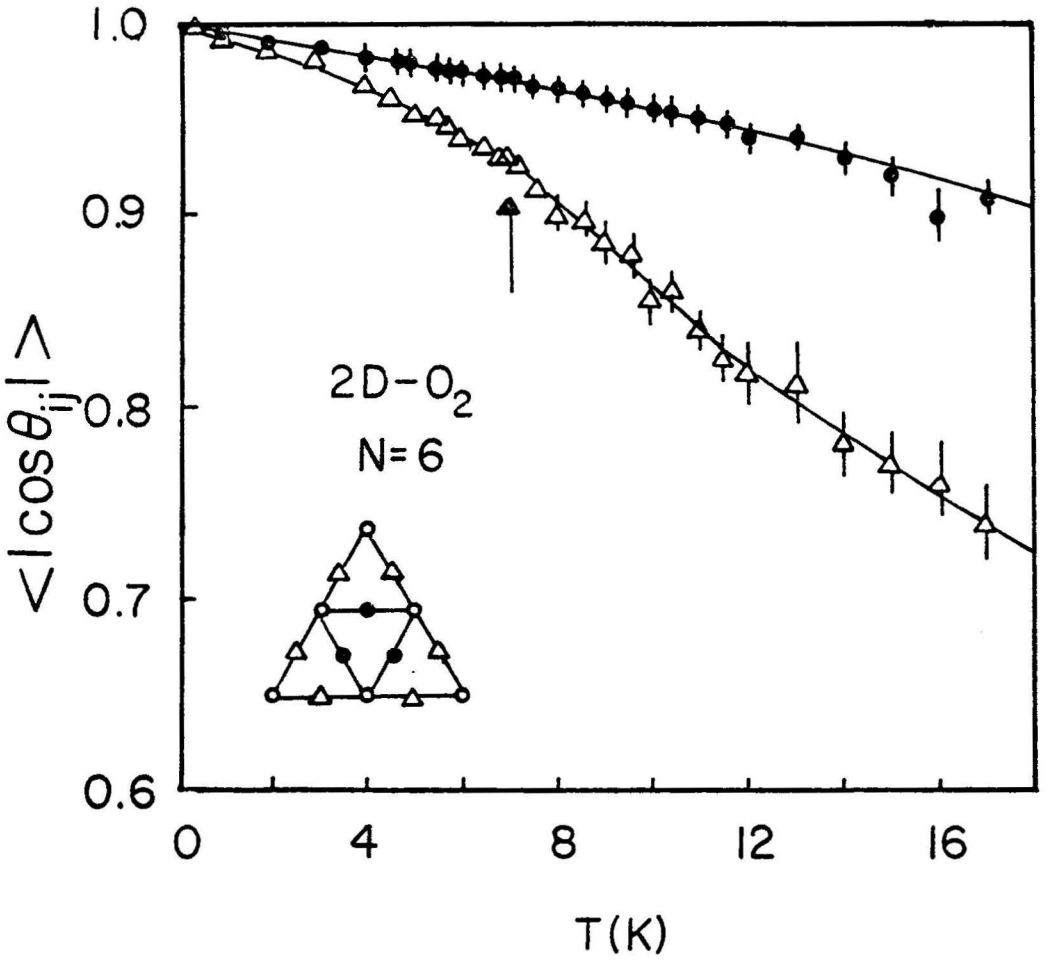

Figure IV-10. $\langle|\cos\theta_{ij}|\rangle$ of nearest neighbor pairs in an isomer of N = 6 β-cluster.

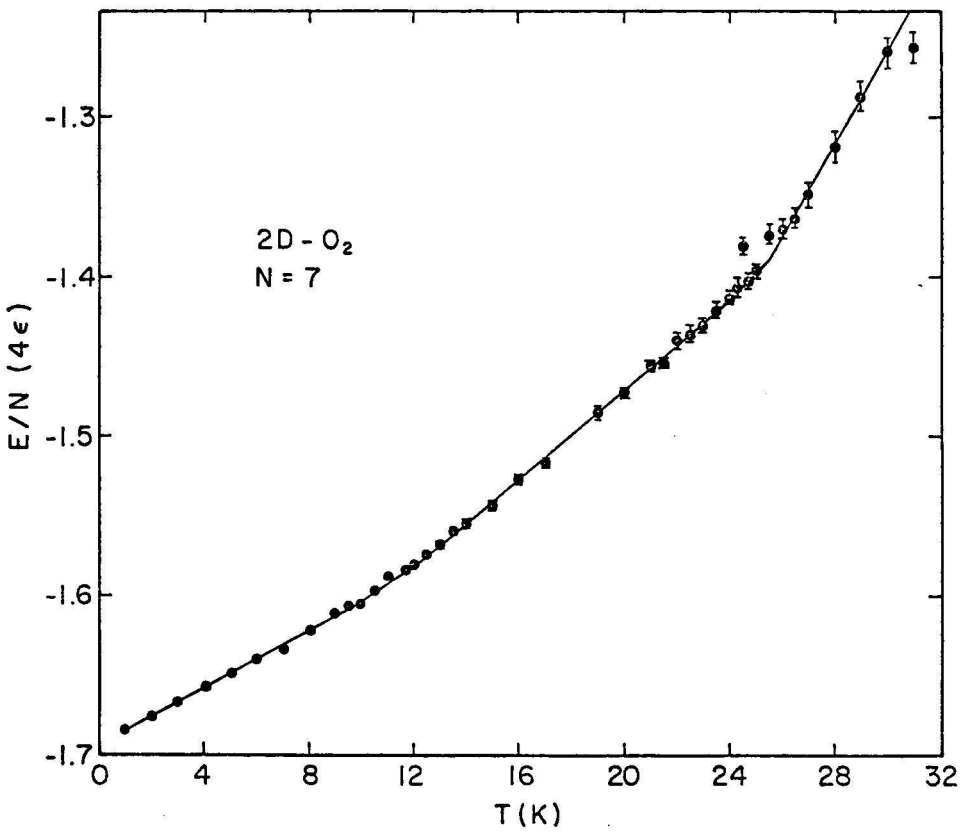

Figure IV-11. Energy per particle for N = 7 β-cluster.

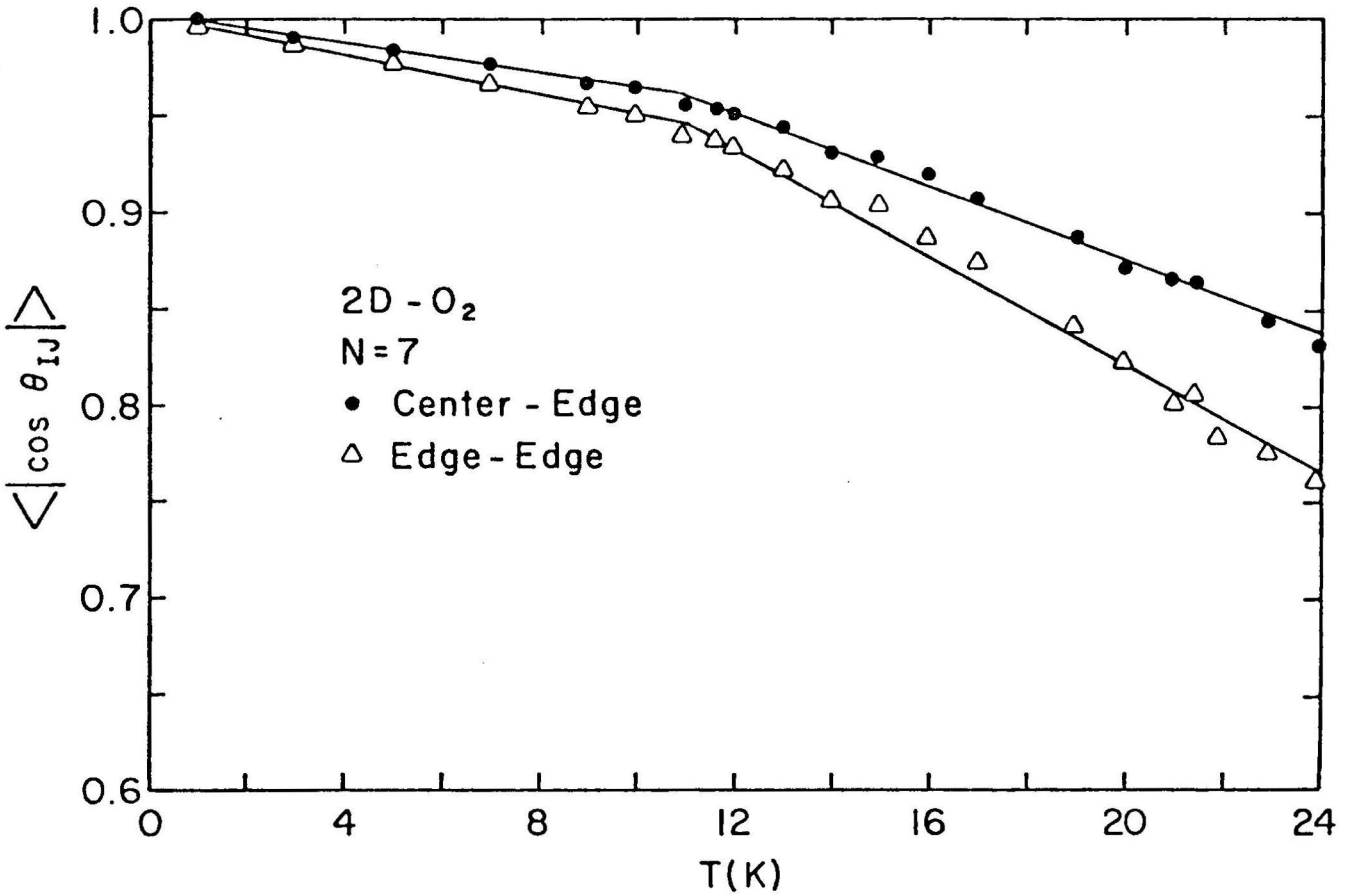

Figure IV-12. $\langle|\cos\theta_{ij}|\rangle$ of nearest neighbor pairs for N = 7 β-cluster.

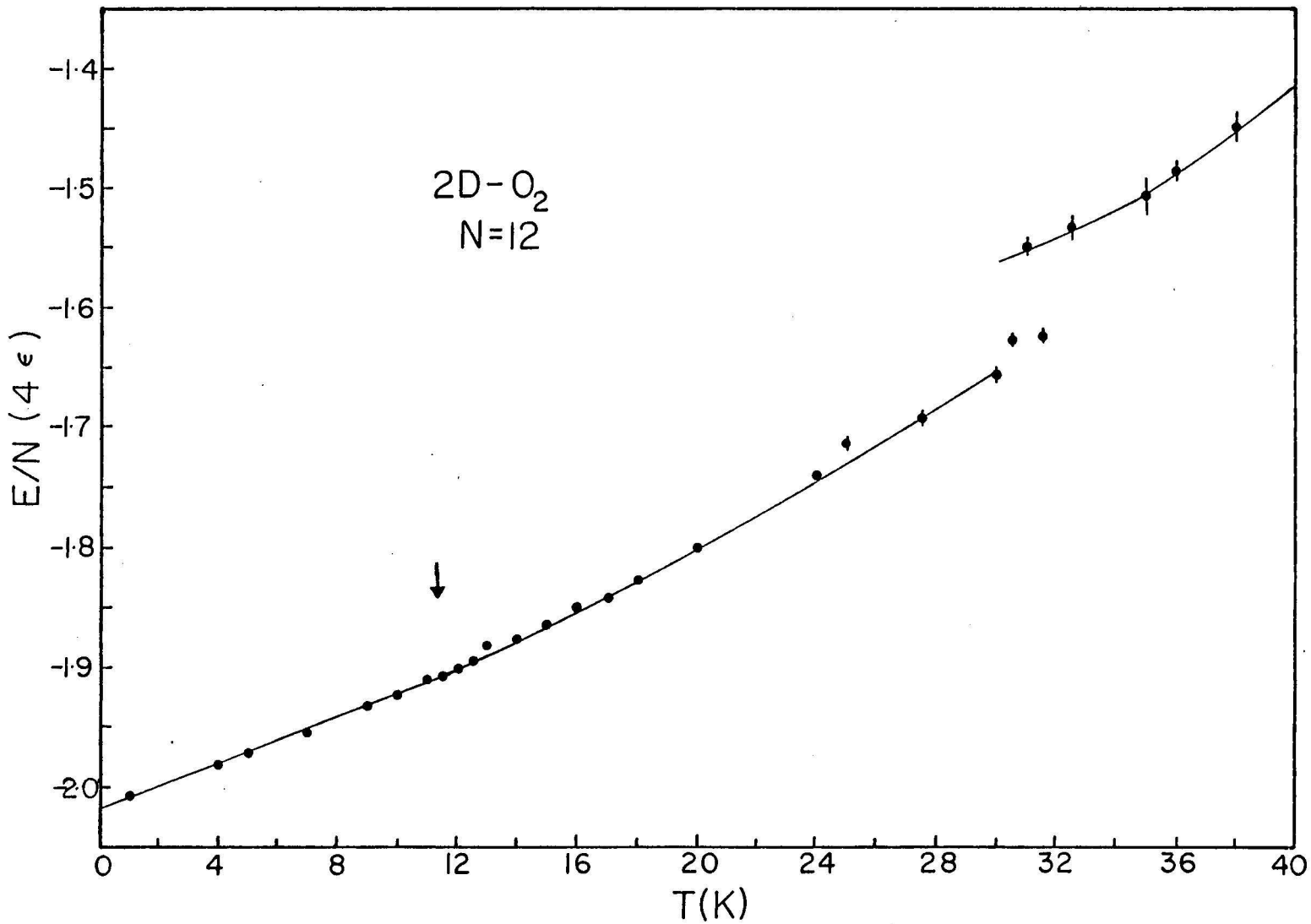

Figure IV-13. Energy per molecule for N = 12 β-cluster.

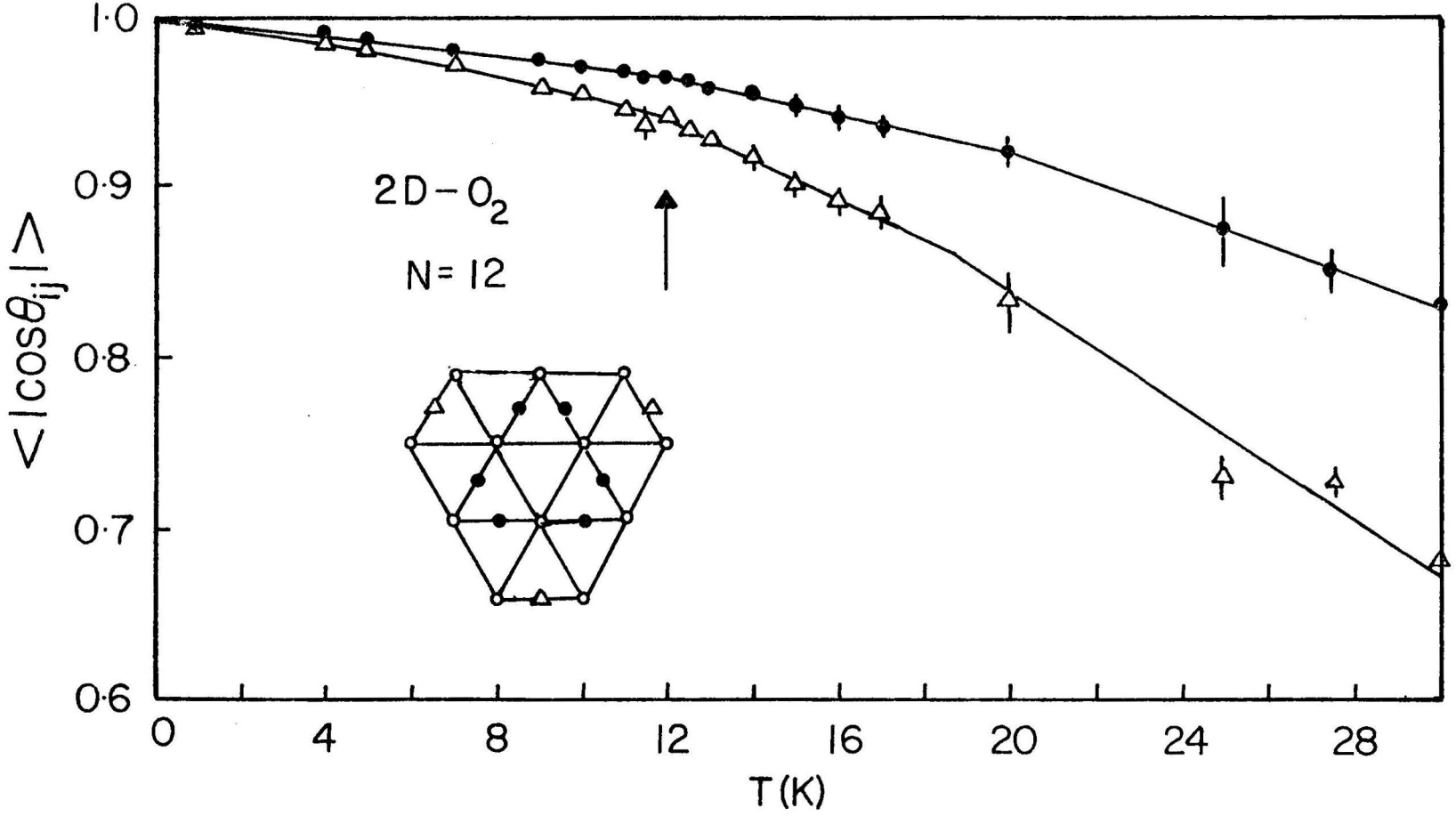

Figure IV-14. $<|\cos\theta_{ij}|>$ for N = 12 β-cluster. The averages of nearest neighbor pairs marked by "Δ" and "•" in insert are plotted with "Δ" and "•" respectively. Error bar indicates spreading of pair values.

Table IV-1. Orientational order-disorder transition temperatures for two-dimensional clusters without surface interaction, (β-clusters).

N	T_{OD2}	T_{OD3}	T_{OD4}
3	5 ± 0.5 K	-	-
4	5 ± 0.5 K	10.5 ± 0.5 K	-
5	5.5 ± 0.5 K	11 ± 0.5 K	14 ± 1 K
6	7 ± 0.5 K	-	14 ± 1 K
7	-	11 ± 0.5 K	-
12	-	11 ± 0.5 K	18 ± 2 K

Figure IV-15. Average nearest neighbor distance in crystallite phase for β-clusters.

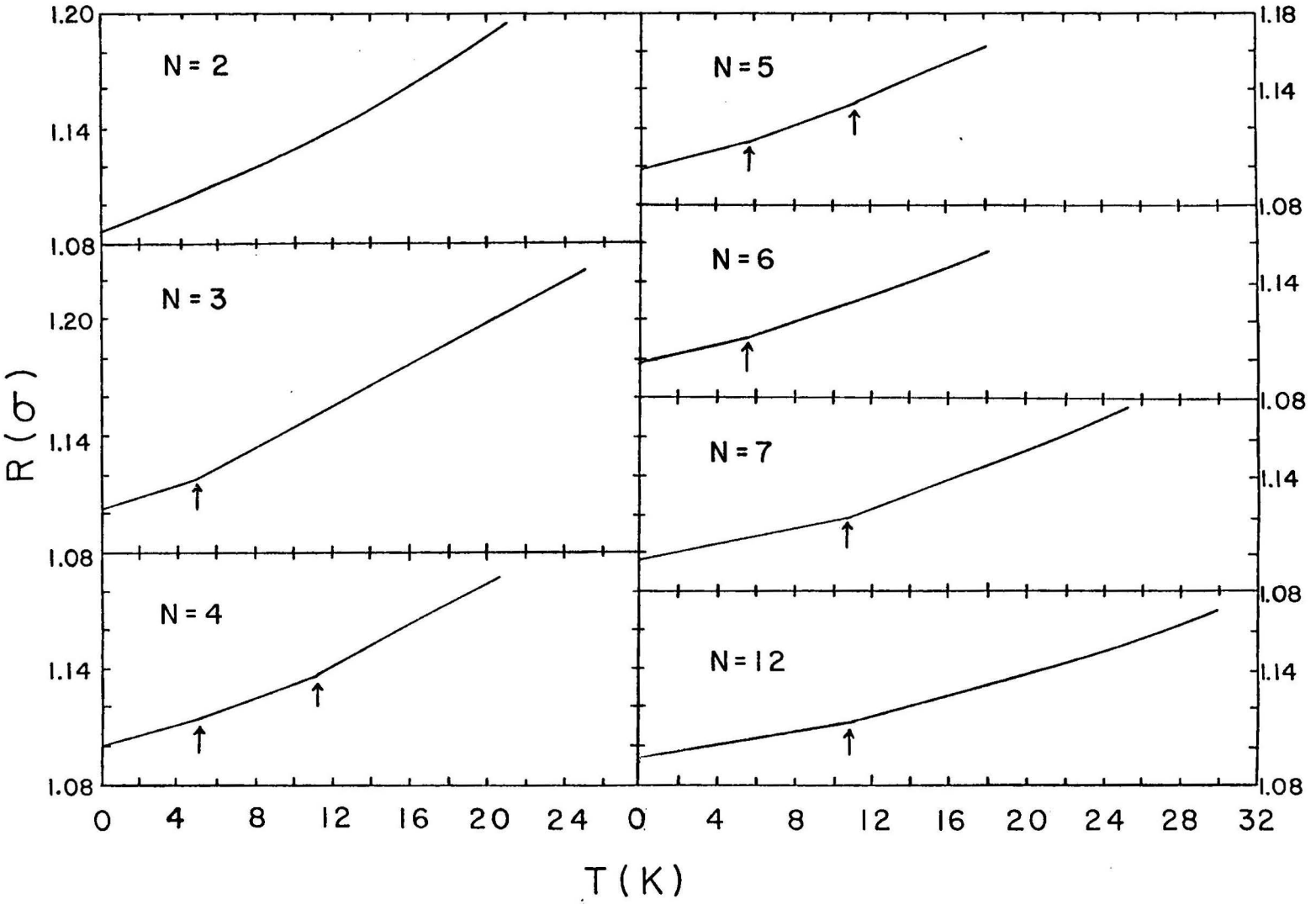
N = 2
N = 3
N = 4
N = 5
N = 6
N = 7
N = 12
R(σ)
T(K)
1.20
1.14
1.08
1.18
0
4
8
12
16
20
24
28
32

the fluctuation becomes so great that the cluster can not maintain its well defined structure. In addition to the structural changes shown along the random walk Markov chain, melting phenomena are also manifested in other physical properties. The energy per molecule of the cluster versus temperature curve shows a sudden change in slope and the average nearest neighbor distance increases abruptly at the melting temperature. Also the bond length fluctuations increase suddenly, and the histogram of thermally averaged bond lengths loses its structural character. All of these changes occur essentially at the same temperature. In a study of three-dimensional rare gas clusters, Etters and Kaelberer[26] have shown that the above physical phenomena are manifestations of the melting transition.

No melting is found for $N = 2$ and $N = 3$ clusters. For $N \geq 4$, the melting phenomena can be detected by all the methods just mentioned. The energy versus temperature curves have been shown in Figs. IV-5, IV-7, IV-9, IV-11, and IV-13 for $N \geq 4$ clusters. For $N = 12$, there is a clear discontinuity at T_M. However the continuity at melting is not obvious in other cases. The energies near T_M for $N = 7$ seems to show a Van der Waal's loop type behavior. Due to the uncertainty of Monte-Carlo calculation, the small discontinuities for $N \leq 7$ at melting temperatures will not be emphasized. The bond lengths, $\langle r_{ij} \rangle$, for all the nearest neighbors within a cluster are averaged and plotted with respect to temperature in Fig. IV-15. For $N \geq 4$, this curve increases monotonically and smoothly as shown until melting. At $T = T_M$, the nearest neighbor, $\langle r_{ij} \rangle$ increase discontinuously to much higher values and with large uncertainty, partly because the nearest neighbors are no longer well defined. The relative bond length

fluctuations, $\Delta r_{ij} = [\langle r_{ij}^2 \rangle - \langle r_{ij} \rangle^2]^{\frac{1}{2}} / \langle r_{ij} \rangle$, for all the nearest neighbor intermolecular bonds are averaged and then plotted with respect to temperature in Fig. IV-16 for various sizes. One can see immediately that the fluctuation increases smoothly with temperature until melting, at which point it drastically increases. The histograms of $\langle r_{ij} \rangle$ are plotted in Figs. IV-17 and IV-18. Taking N = 7 as an example, the histogram remains essentially the same for $0 \leq T \leq 25$ K except for some shifting, which represents the thermal expansion. At T = 25.5 K , the longer bond length peaks begin to broaden indicating a loss of long range order. At T = 26 K the historgram no longer has the character of those at lower temperature. These anomalies happen at essentially the same temperature.

Considering all information, T_M = 20 K, 18 K, 18 K, 25 K, and 30 K for N = 4,5,6,7, and 12, respectively. With uncertainties, the melting temperatures are plotted in Fig. IV-19.

The melting temperature for the N = 5 and N = 6 clusters are lower than that for the N = 4 cluster, because some low energy saddle points exist between the energy minima in the energy-configuration surface. The structures then are able to distort with relative ease into several equivalent metastable states. This phenomenon is illustrated in Fig. IV-20. When one molecule can move through a low energy path from one minimum to another, the bond distance, bond fluctuation and energy associated with this moledule will change significantly such that the plots of these quantities versus temperature will no longer be smooth curves. Looking at the bond length flucutations again, one can see that for N = 4,7, and 12 the relative fluctuations all increase to approximately 8% at the melting temperatures

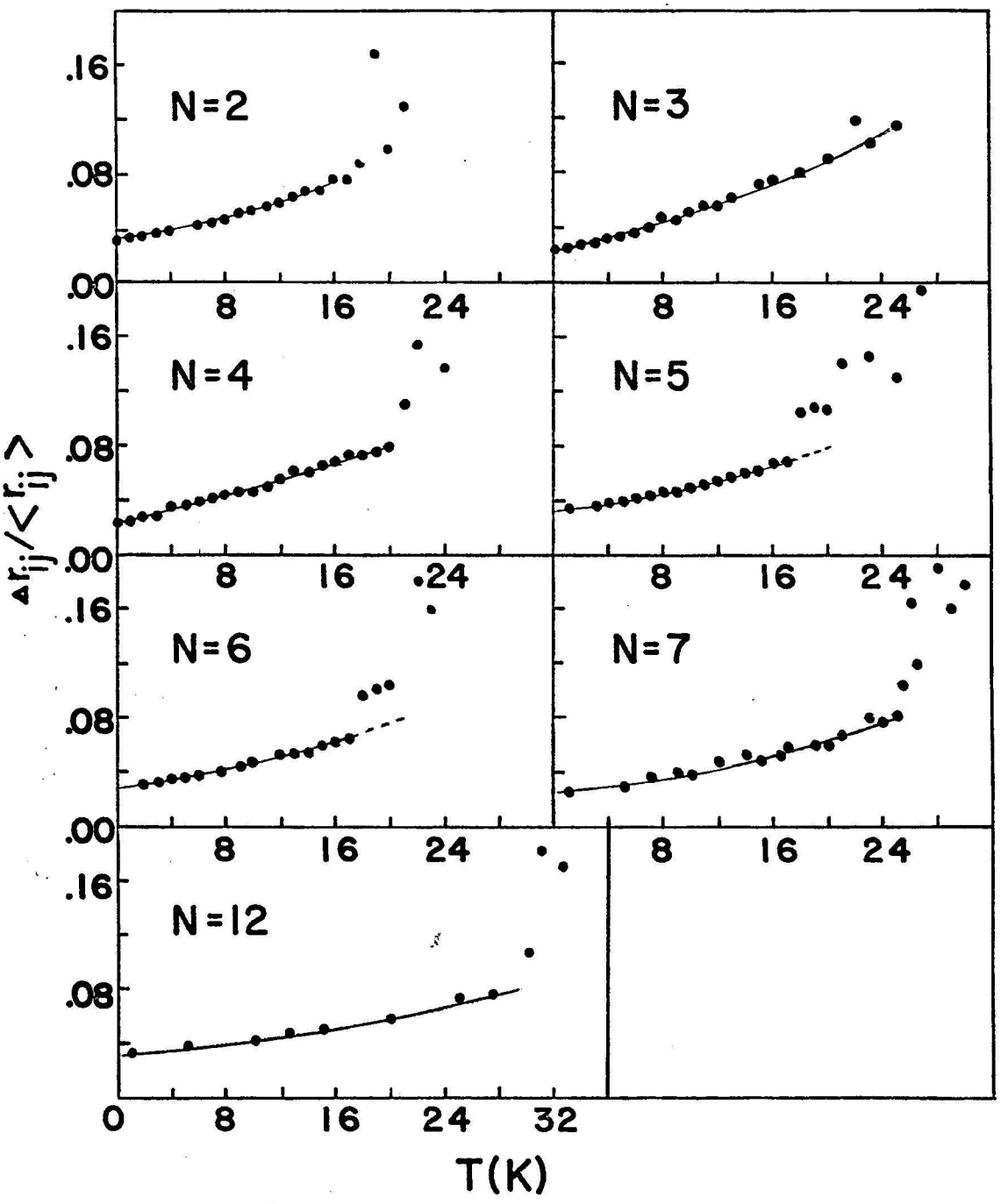

Figure IV-16. Relative nearest neighbor bond length fluctuation. $\Delta\langle r_{ij}\rangle/\langle r_{ij}\rangle = [\langle r_{ij}^2\rangle - \langle r_{ij}\rangle^2]^{1/2}/\langle r_{ij}\rangle$ for all nearest neighbor bonds in a β-cluster are averaged and plotted versus temperature.

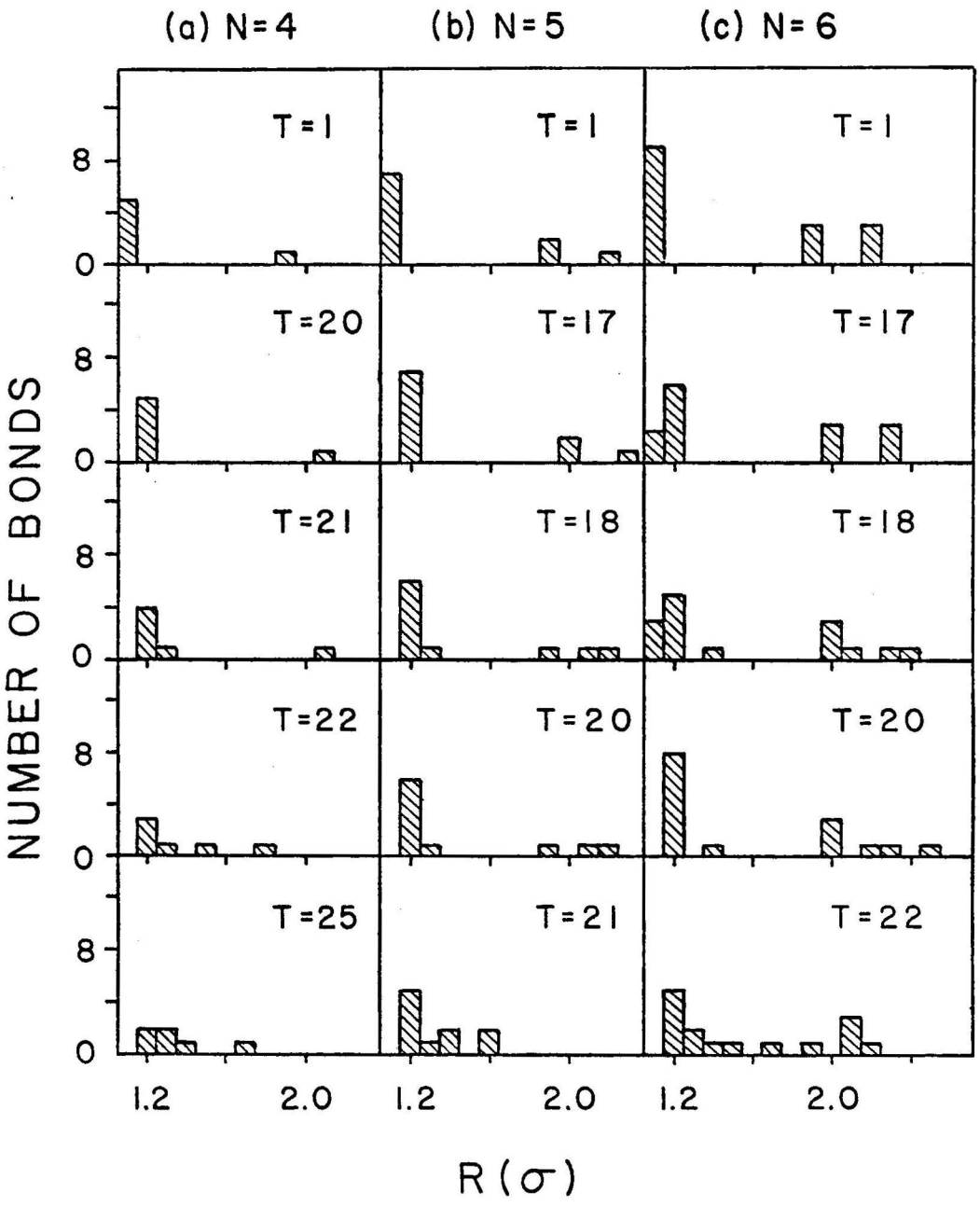

Figure IV-17. Historgrams of average bond lengths for (a) N = 4 , (b) N = 5 , (c) N = 6 (equilateral triangle) β-clusters, at various temperatures.

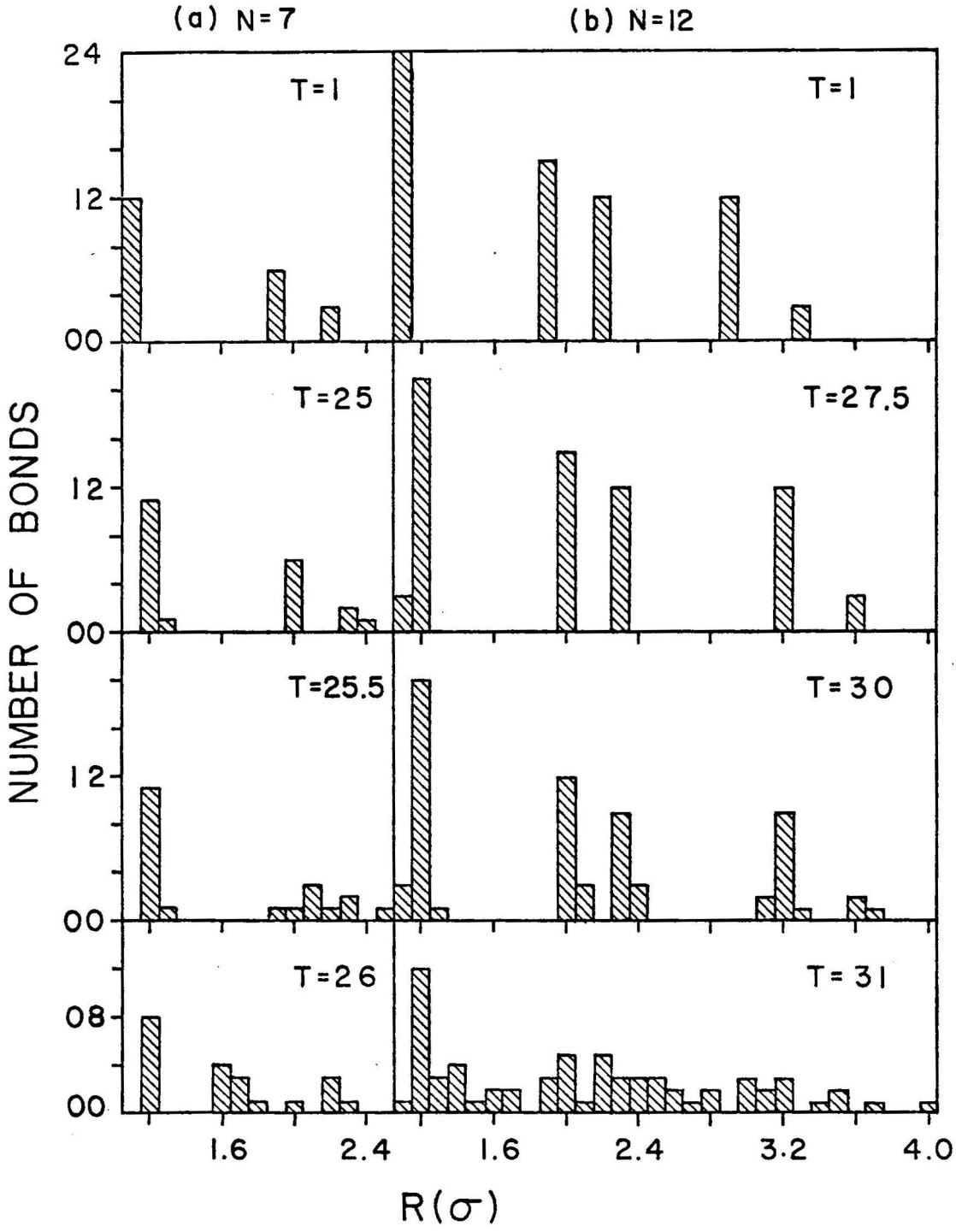

Figure IV-18. Histograms of average bond lengths for (a) N = 7 , and (b) N = 12 β-clusters, at various temperatures.

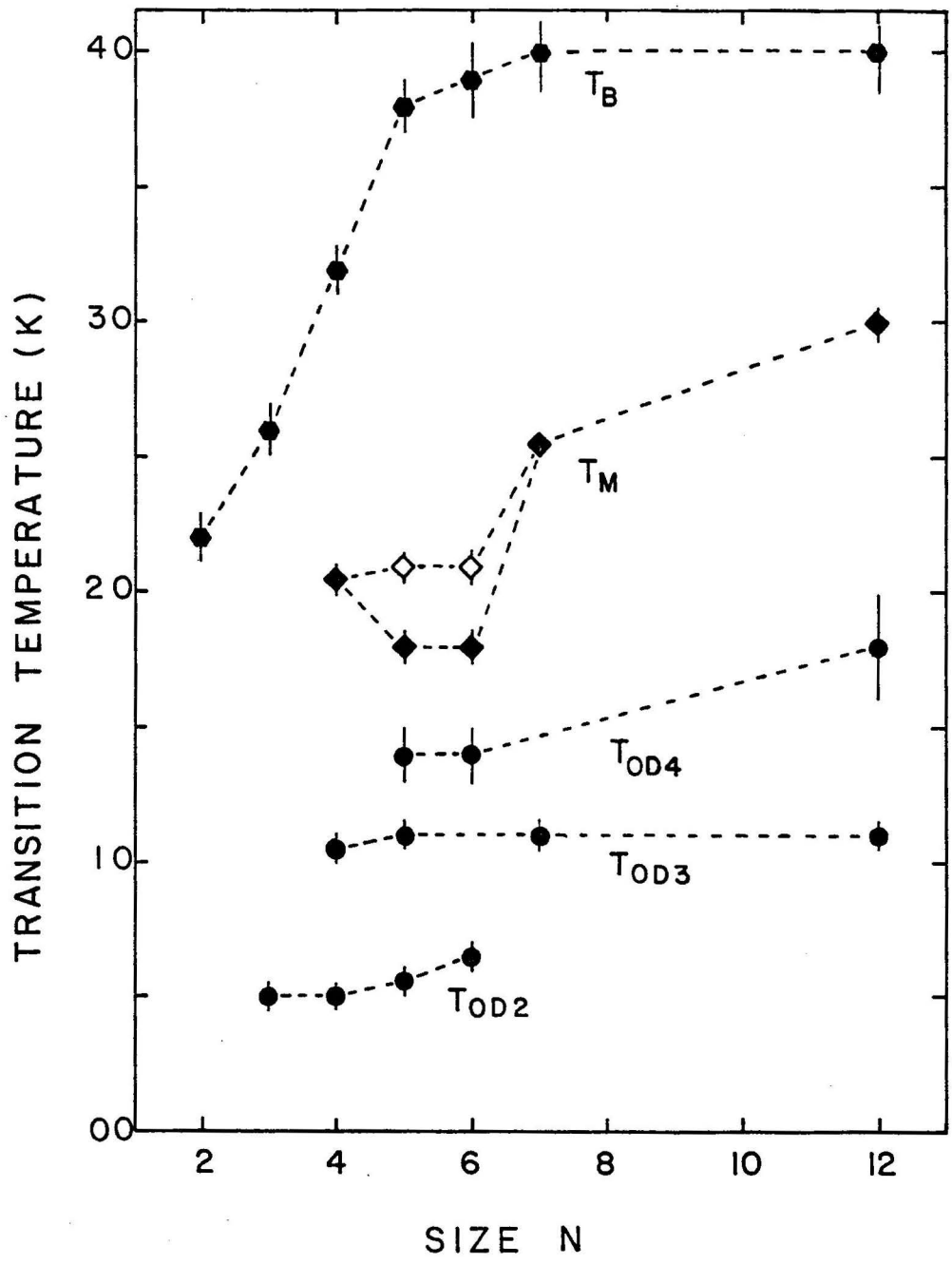

Figure IV-19. Orientational order-disorder transition (T_{OD2}, T_{OD3}, T_{OD4}), melting (T_M), and dissociation (T_B) temperatures for β-clusters.

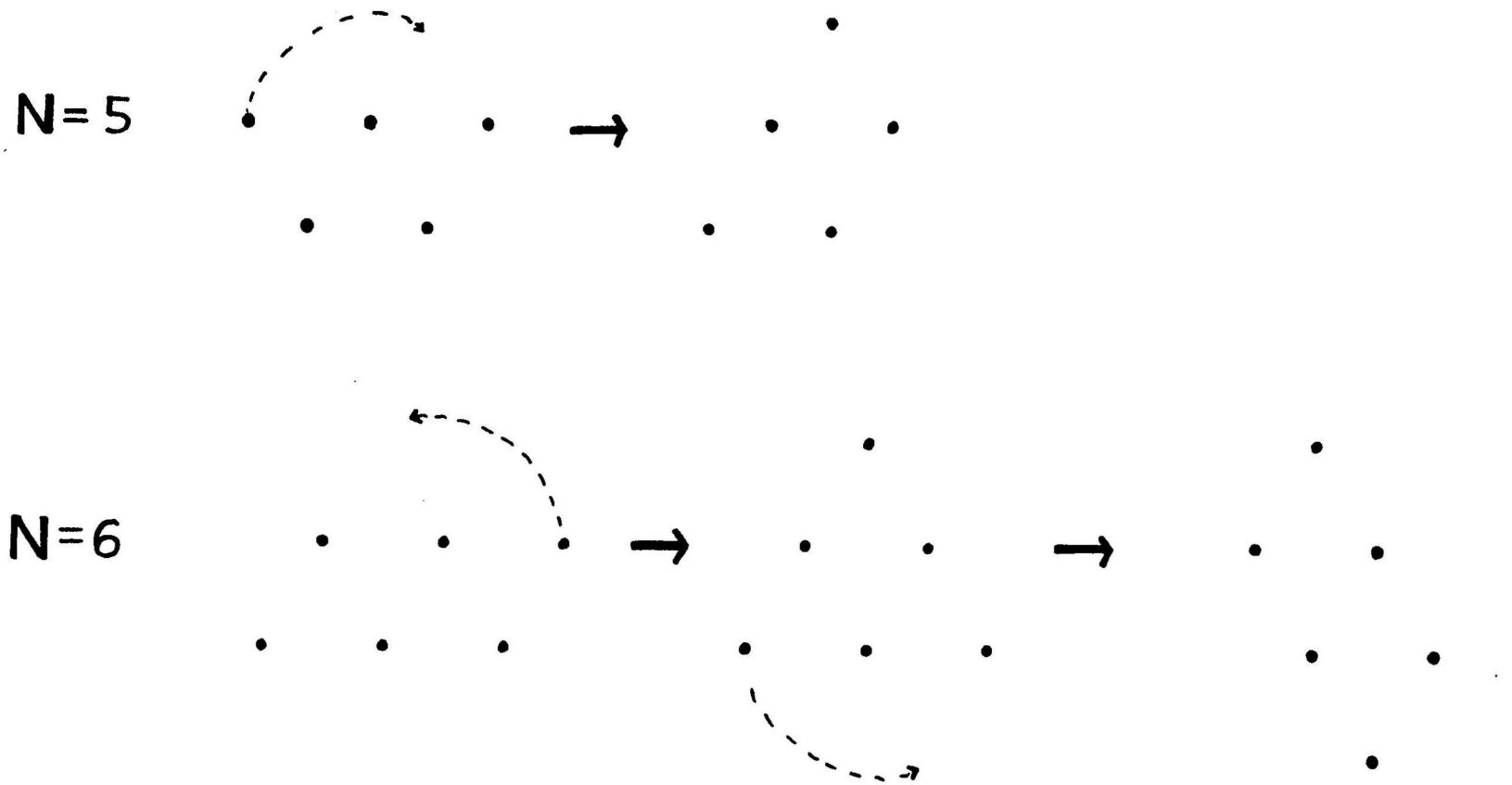

Figure IV-20. A sketch for N = 5 (a) and N = 6 (b) β- clusters moving between degenerate or nearly degenerate structural states.

and then suddenly increase to much greater values. For the $N = 5$ and $N = 6$, the bond fluctuations increase abruptly at the melting temperatures, but they do not increase as much as those for the other sizes (i.e., $N = 4$, 7, and 12). If we take an approach similar to the Lindemann melting criterion[28] and define melting at $\Delta r_{ij}/\langle r_{ij}\rangle = 8\%$, the melting temperatures for $N = 5$ and $N = 6$ are both about 21 K. In fact, for these two cluster sizes, the fluctuations do increase dramatically at $T \simeq 21$ K, and the bond length histogram shows that the short range order for nearest neighbors bond lengths is also kept until $T \simeq 21$ K. Therefore, it is concluded that the melting phenomena for $N = 5$ and $N = 6$ occur in two stages. In the beginning, the energetically degenerate structural states or nearly degenerate states are mixed. At the end of the melting process, the structural order is totally lost.

Section IV-A-4, Dissociation Transitions

As temperature increases, the fluid like cluster has more energy to expand, and the probability for an individual molecule to escape increases. The dissociation process and identification for three-dimensional rare gas clusters have been discussed in detail by Etters and Kaelberer.[26] The same method is used here. The dissociation process manifests itself gradually in this study. This is a temperature range in which dissociation appears frequently, yet very often the cluster still remains in the liquid phase. The dissociation temperature, T_B, is taken to be the temperature beyond which dissociation always appears. All the T_B's for the cluster sizes we studied and their uncertainties are shown in Fig. IV-19.

Section IV-A-5, Summary

Two-dimensional O_2 clusters with $2 \leq N \leq 12$ without surface interaction are studied. The structures are basically formed by joining together equilateral triangles with molecules oriented perpendicular to the cluster plane.

The $N = 2$ dimer exhibits only a dissociation transition. The $N = 3$ trimer has an orientational order-disorder transition in addition to dissociation. Clusters with $N \geq 4$ show orientational order-disorder transitions in the crystallite state, melting, and dissociation transitions. There are more than one orientational order-disorder transition in some sizes of clusters because there exist inequivalent sites. The molecules with two nearest neighbors become disordered at lower temperatures than those with three nearest neighbors and so on. The molecules with five or six nearest neighbors do not show any orientational disorder prior to melting. All of the transitions and their uncertainties are plotted in Fig. IV-19 verus N. The melting process for $N = 5$ and 6 includes two stages of structural changes. The beginning and end of this process are marked by "♦" and "◊" in Fig. IV-19. Examining the trend for the melting temperature in Fig. IV-19, it is clear that T_M approaches 35 K asymptotically. This is an excellent agreement with experimental data[2,8] (Fig. I-3).

Section IV-B, Adsorbed Oxygen Clusters on Graphite with Atom-Atom Adsorption Interaction

In this section, results of a Monte-Carlo study on adsorbed oxygen clusters of sizes $2 \leq N \leq 7$ will be presented. A Lennard-Jones 6-12 atom-atom potential is used for oxygen-graphite interaction (Eqs. II-16,

II-18, II-20, and II-21). This potential keeps the oxygen atoms approximately at the same distance from the substrate. Planar structures with the molecular axes parallel to the surface result. These structures are analogous to that of δ-film, the clusters studied in this section are then named δ-clusters.

With the extra orientational degrees of freedom for the planar molecules, the number of isomers increases drastically compared to the β-clusters discussed in section A.

At low temperatures, the clusters librate about their equilibrium orientations. The libration increases with temperature until the degenerate and isomeric states mix. The molecules then undergo planar rotation, even though their motions are still hindered with several preferred orientations. This initiates the orientationally disordered phase. With increasing temperature, the molecules rotate more freely, approaching planar free rotor states. The melting and dissociation criteria are the same as for β-clusters studied in section IV-A.

In the following, the structures, registry to substrate, orientational order-disorder phase transitions, melting, and dissociation transitions will be described.

Section IV-B-1, Registry to the Substrate

Registry is used here to describe the mobility of a cluster relative to the substrate. Because of the texture of the substrate surface, the adsorbed molecules are strongly attracted to certain points on substrate. One expects that the cluster will be locked on to the surface at some locations with certain orientations when the temperature is low enough and if the zero point motion is negligible.

However, the graphite surface is quite smooth, and registry of a cluster may not be easily detected experimentally. At higher temperatures, the thermal energy may be sufficient for the O_2 molecules to escape the graphite surface trapping centers and migration of the cluster along the substrate then becomes possible.

There is evidence showing that the $N = 3$ clusters register. The total energy, including the internal energy of cluster and the adsorption energy between the cluster and the graphite, increases discontinuously at about 3 K . This discontinuity is due to the adsorption energy only. The internal energy of the cluster changes smoothly around 3 K (Fig. IV-21). The fluctuations of molecular center positions along x-y plane, $\Delta r_i = [\langle x_i^2 \rangle - \langle x_i \rangle^2 + \langle y_i^2 \rangle - \langle y_i \rangle^2]^{\frac{1}{2}}$, $i = 1,2,3$, are averaged and plotted in Fig. IV-22 with respect to temperature. At $T < 3$ K , the small fluctuations indicate that each molecule is locked onto the surface. For $T > 3$ K , the large positional fluctuations show that the cluster as a whole can move on the substrate surface. The bond length fluctuations, $\Delta r_{ij}/\langle r_{ij} \rangle$, versus temperature as in Fig. IV-22 also changes discontinuously at $T = 3$ K , because the graphite trapping centers, which attract the molecules in registry and hence keeps bond length stable at low temperatures, are overcomed by thermal fluctuations.

The Δr_i and Δr_{ij} values also indicate that the $N = 2,6$, and 7 clusters manifest registry at very low temperatures, but this is not reflected in the adsorption energies as it is for $N = 3$. In Fig. IV-23, Δr_i and $\Delta r_{ij}/\langle r_{ij} \rangle$ versus temperature curves are shown for $N = 7$. The abrupt changes around 3.5 K for both Δr_i and $\Delta r_{ij}/\langle r_{ij} \rangle$ indicate an in-registry to out-of-registry transition for $N = 7$ by

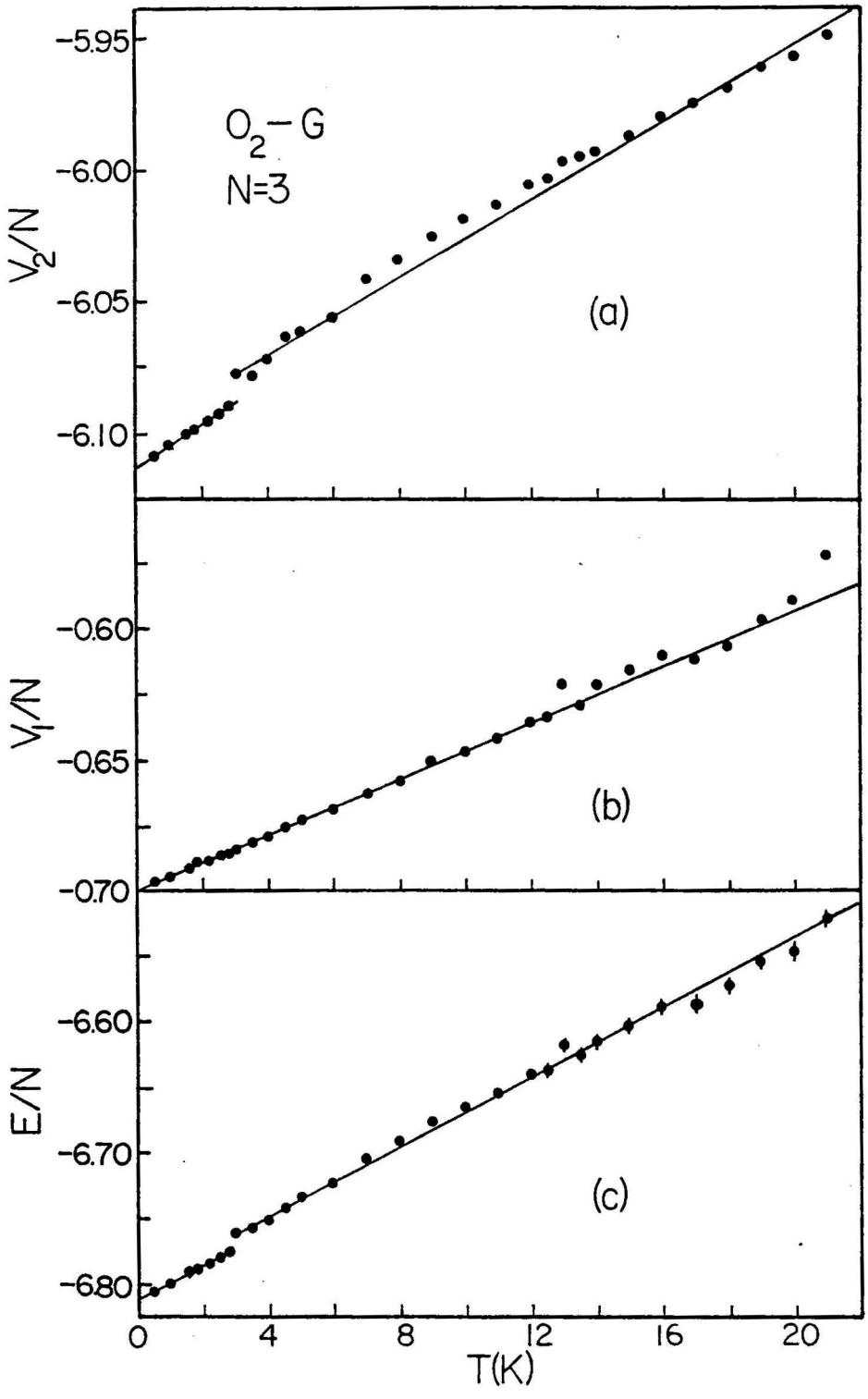

Figure IV-21. Adsorption energy (a), internal energy (b), and total energy (c) per molecule for N = 3 δ-cluster.

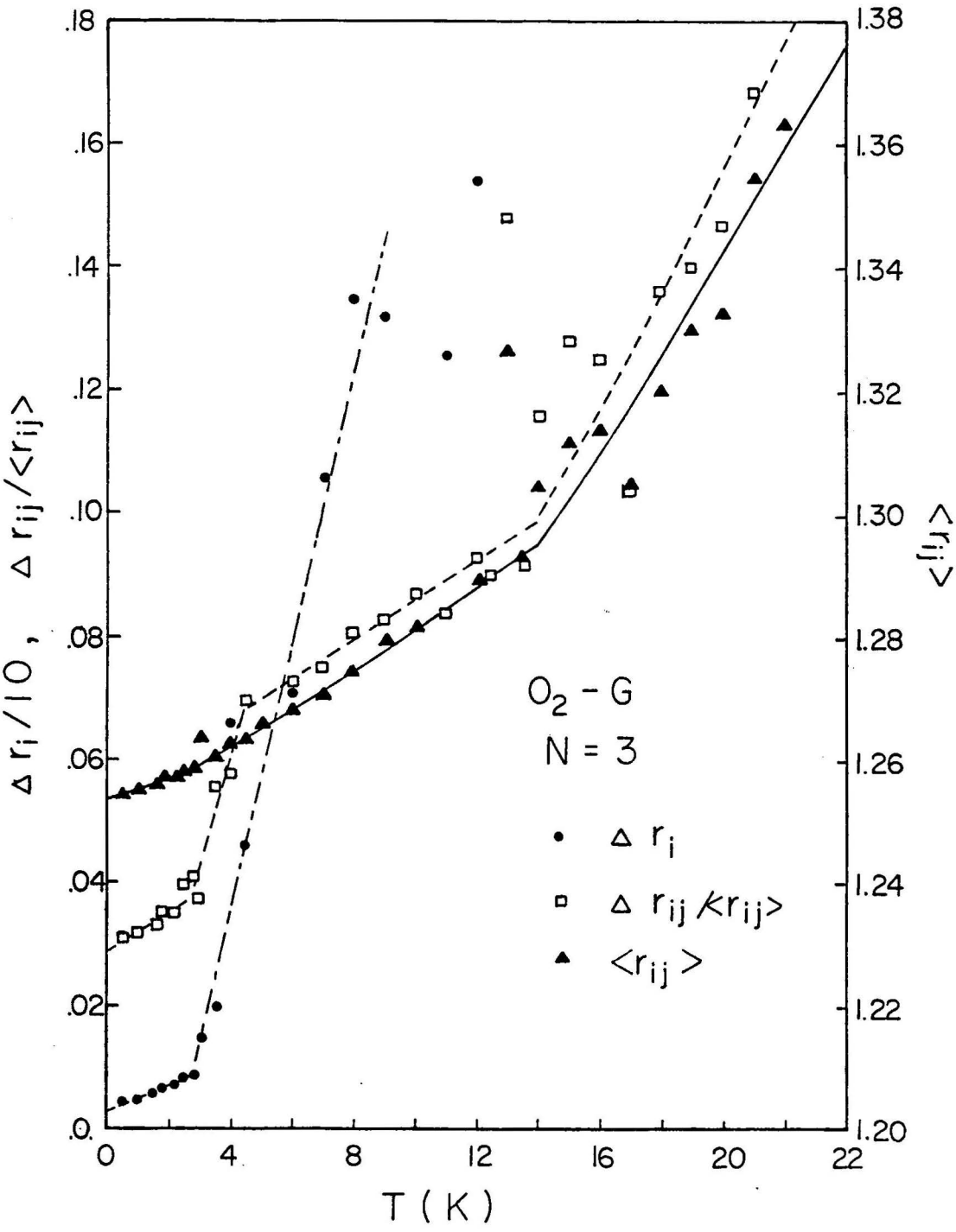

Figure IV-22. Average of positional fluctuation (Δr_i) , relative bond length fluctuation ($\Delta r_{ij}/\langle r_{ij}\rangle$) , and bond length ($\langle r_{ij}\rangle$) for N = 3 δ-cluster.

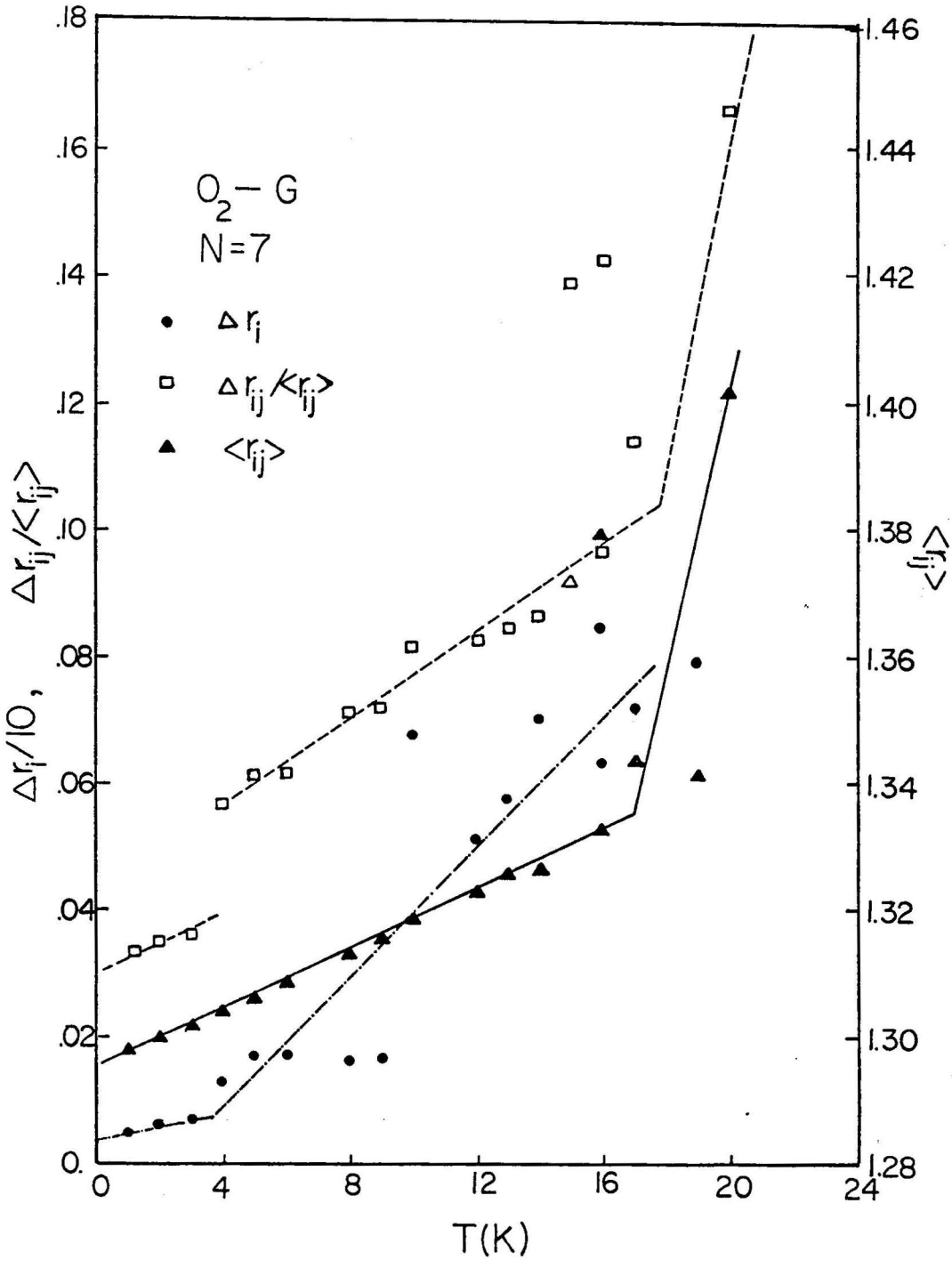

Figure IV-23. Averages of positional fluctuation (Δr_i), relative nearest neighbor bond length fluctuation ($\Delta r_{ij}/\langle r_{ij}\rangle$), and nearest neighbors bond length ($\langle r_{ij}\rangle$) for N = 7 δ-cluster.

the same discussion just mentioned for $N = 3$. The other slope changes in Fig. IV-22 and Fig. IV-23 are associated with transitions discussed later.

There are no evidences of registry of $N = 4$ or 5. This is probably because the symmetries of $N = 4$ and $N = 5$ clusters do not match well with the graphite surface symmetry.

Section IV-B-2, Structures and Orientational Phase Transitions

The center of mass structures are similar to those for β-clusters. However, the orientation forces produce distortions, because the the minimum energy separation of a pair of O_2 depends on the molecular orientations.

The $N = 2$ dimer has a parallel structure. That is, the two molecules are parallel to each other and perpendicular to the intermolecular bond. Two structures are found for $N = 3$, as illustrated in Figs. IV-24(a) and (b). The equilateral triangle is found in the low temperature registered phase, while the irregular nonregistered structure appears at higher temperatures. The second structure with its mirror image forms the structure for $N = 4$ clusters shown in Fig. IV-24(c). For $N \geq 5$, the detailed structures are very complicated and many isomeric states exist with small differences in individual molecular orientations. In Table IV-2, the positions and orientations of the molecules are given.

The molecules in the $N = 2$ dimer are parallel to each other and the method used to identify the orientational order-disorder transition for $N = 2$ is identical to that described in section IV-A for β-clusters. The orientational order-disorder transition for the $N = 3$

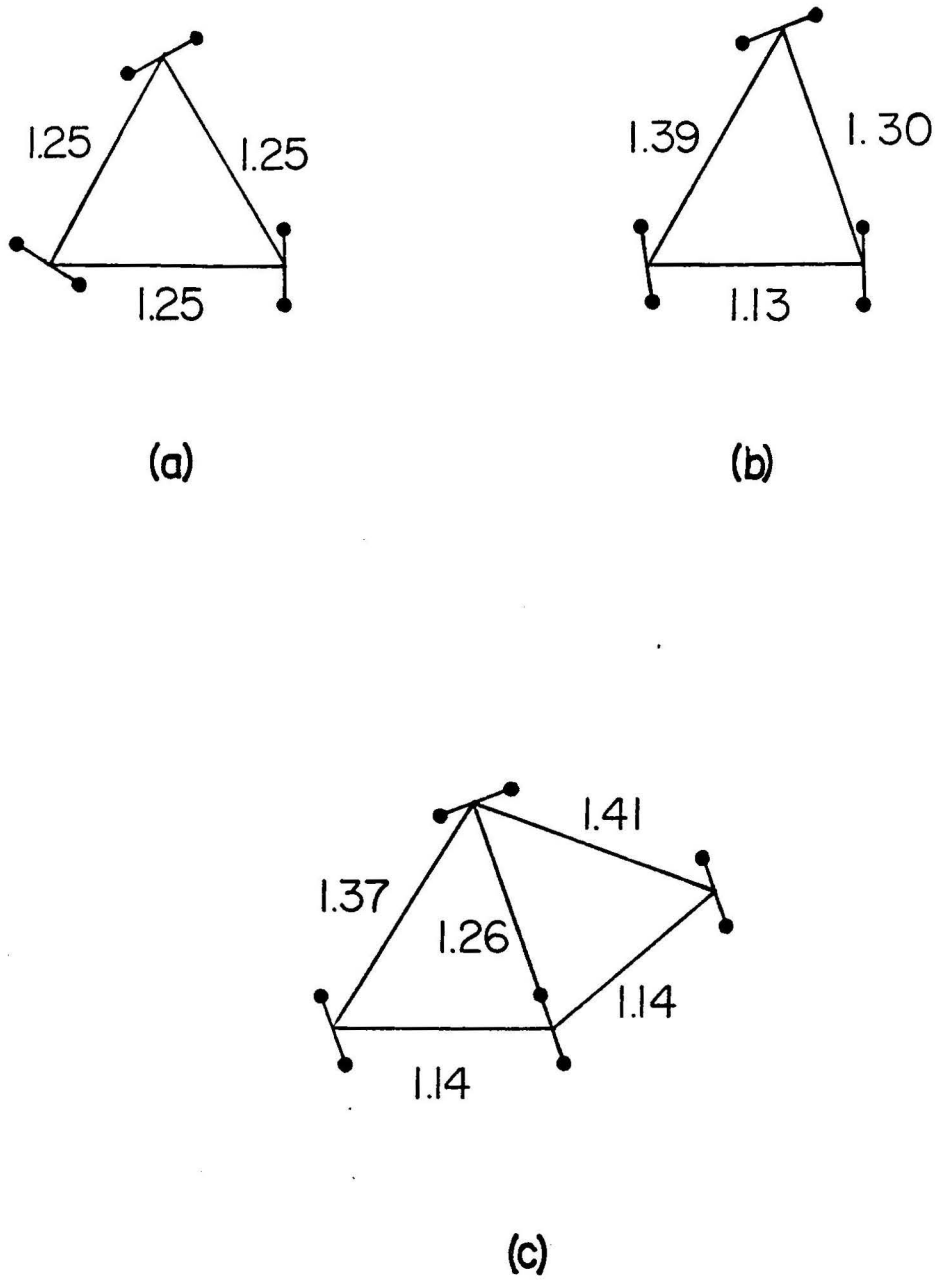

Figure IV-24. Sketches for the two isomers for N = 3 δ-cluster and (a,b) N = 4 δ-cluster (c).

Table II-2. The configurations for δ-clusters. All molecules are parallel to the graphite surface. The distance of each molecule from the graphite surface is 1.05. For each molecule, two variables are used to specify the x and y coordinates of its center of mass and one variable for specifying the azimuth angle of the molecular axis on the x-y plane. For easy reading, each configuration has been transferred to a coordinate system with molecule 1 sitting on the origin, and molecule 2 on x'-axis. The three numbers in a pair of parentheses are x' , y' coordinates of the molecular center and the angle of the molecular axis from the x'-axis in radians, respectively.

N	(x', y', ϕ')			
2	(0, 0, 1.57)	(1.12, 0, 1.57)		
3(a)	(0, 0, 1.57)	(1.25, 0, 0.52)	(0.64, 1.08, -0.52)	
3(b)	(0, 0, -0.69)	(1.39, 0, 0.70)	(0.54, 0.99, -0.63)	
4	(0, 0, -1.22)	(1.14, 0, -1.22)	(0.71, 1.18, 0.35)	(2.01, 0.73, -1.22)
5	(0, 0, 0.49) (0.59, -0.96, 0.51	(1.41, 0, -0.60)	(0.83, 1.13, 0.40)	(-0.44, 1.16, 1.30)
6	(0, 0, 0.57) (0.83, -0.94, -0.52)	(1.41, 0, -0.54) (-0.39, 1.18, 1.33)	(0.72, 1.24, 1.42)	(1.95, 0.96, -0.60)
7	(0, 0, -0.67) (-0.53, 1.31, -0.69)	(1.38, 0, 0.65) (1.46, 2.22, 0.24)	(0.69, 1.04, 1.51) (0.20, 2.33, 1.36)	(1.94, 1.11, -0.36)

trimer is accompanied by an in-registry to out-of-registry transition. For $T < 3$ K, it is a registered equilateral triangle with $\theta_{ij} = 2\pi/3$, $i,j = 1,2,3$, and, for $T > 3$ K, the average configuration for centers of mass is also a equilateral triangle, however, the instantaneous configurations are mostly like the irrigular triangle as shown in Fig. IV-24(b). With enough librational freedom, several degenerate orientational states mix. Each bond varies in length depending on the molecular orientations, with an equilateral triangle being the average result. A similar situation exists for $N = 4$ at $T \simeq 4$ K. For $T > 4$ K, there is sufficient libration for molecules 2 and 3 (see Fig. IV-24(c)) to exchange their orientations, resulting in a mirror image structure. When this occurs, the average center-of-mass configuration becomes a regular 60^{o} rhombus, and the bond length fluctuations increase drastically.

Besides the mixing of degenerate states, the orientational disorder is initially due to the mixing of several nearly degenerate states. That is, isomeric states with different orientational configurations but with energies very close together. This is particularly true for $N = 5$.

There are several ways by which we can identify the orientational transitions for $N \geq 3$. First, the bond length fluctuation versus temperature curve has an abrupt increase at a temperature, T_{OD}. This is because the orientational and translational degrees of freedom are coupled. Secondly, the average bond length histogram becomes narrowly peaked and shows the features of those clusters formed with equilateral triangles at the same temperature. The reasons for this have just been discussed for $N = 3$ and $N = 4$. To illustrate, the historgrams for

$N = 7$ and $N = 4$ are shown in Fig. IV-25 for several temperatures. Finally, several instantaneous configurations along random walk chain are examined for each temperature, so the way structures change can be monitored. It has been found that the molecular orientations change more rapdily for $T \geq T_{OD}$. The energy versus temperature curves for these clusters usually do not show clear changes at the orientational transitions.

The $N = 5$ cluster has many energetically nearly degenerate isomeric states. It is found that these states are already mixed at 1 K.

The $N = 6$ cluster forms a distorted triangle. The bond length histogram shows that the orientational disorder transition occurs at $T_{OD} \simeq 3$ K. After the onset of orientational disorder, the three-fold symmetry is retained for the thermally averaged structure, although the three nearest neighbor bonds among the three middle molecules are longer than the other six nearest neighbor bonds.

From the bond length histograms for the $N = 7$ clusters (Fig. IV-25(b)), it is apparent that the average configuration becomes a perfect hexagon at $T \geq 8$ K.

At $T > T_{OD}$, the molecules become hindered rotors on the cluster plane with high probabilities at several preferred orientations. With increasing temperature, the molecules become more nearly two-dimensional free rotors. In Figs. IV-26 and 27, $\langle \cos \theta_{ij} \rangle$, $\langle \cos^2 \theta_{ij} \rangle$ and $\langle |\cos \theta_{ij}| \rangle$ are plotted against temperature for the $N = 4$ cluster. For an ideal two-dimenstional free rotor, these quantities are 0, 0.5, and $2/\pi$, respectively, which are shown as horizontal lines in the graphes. The vertical lines at $T = 15$ K shows the melting temperature.

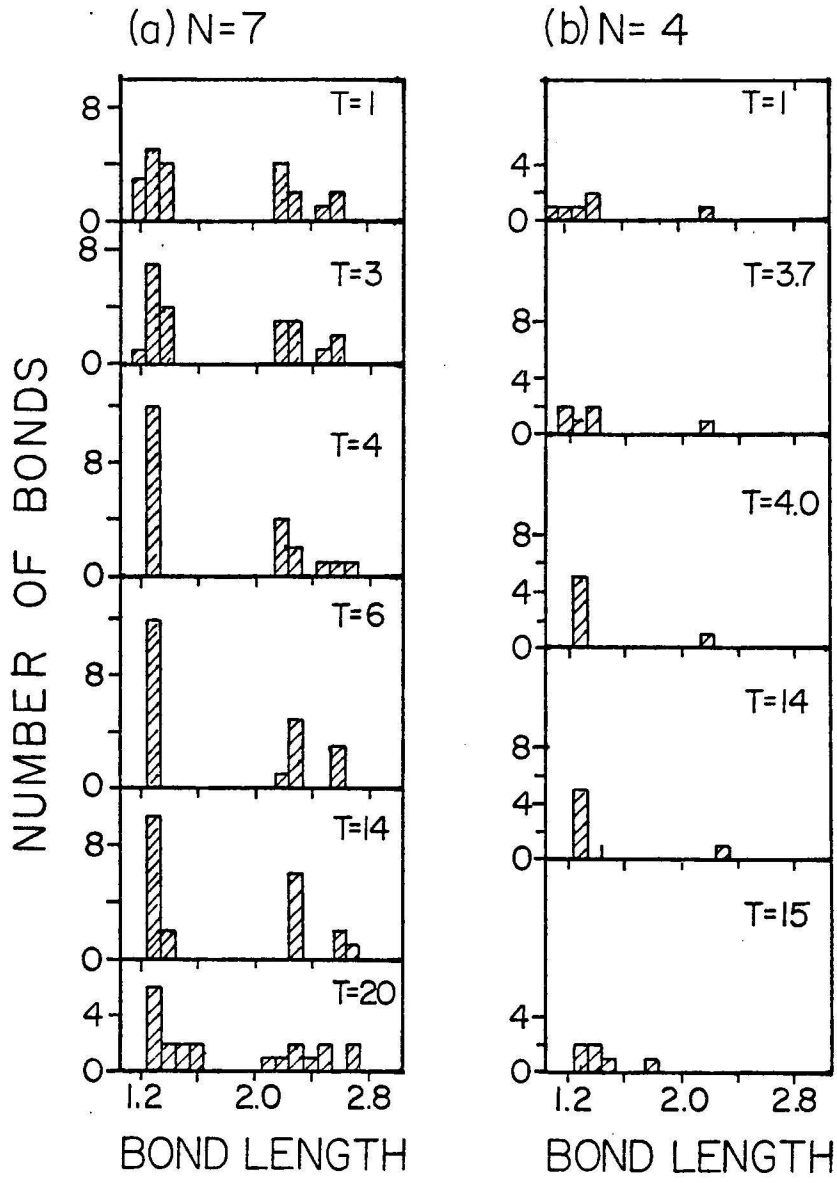

Figure IV-25. Bond length histograms for (a) N = 7 and (b) N = 4 δ-clusters.

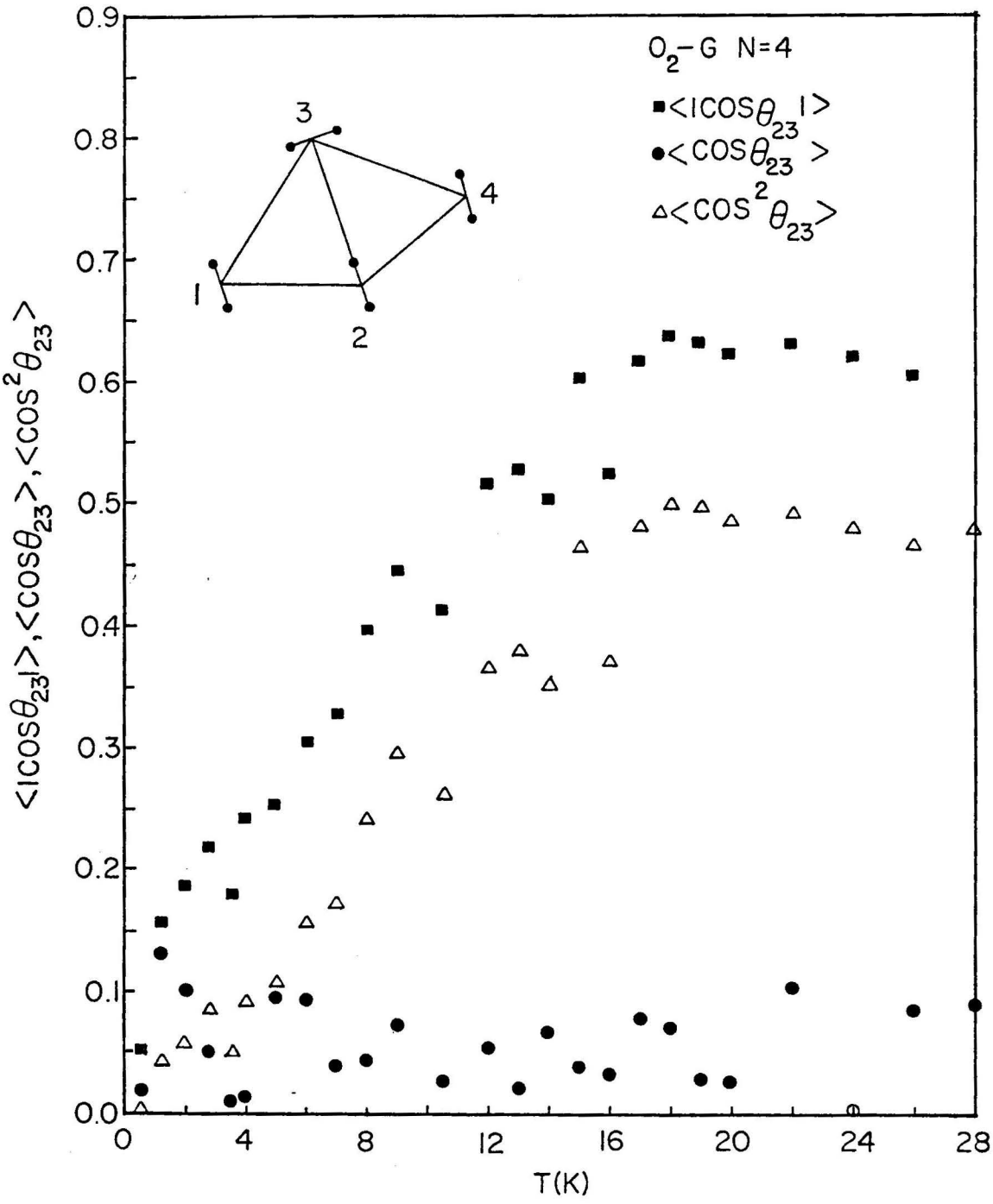

Figure IV-26. $\langle|\cos\theta_{23}|\rangle$, $\langle\cos\theta_{23}\rangle$, and $\cos^2\theta_{23}$ in N = 4 δ-cluster.

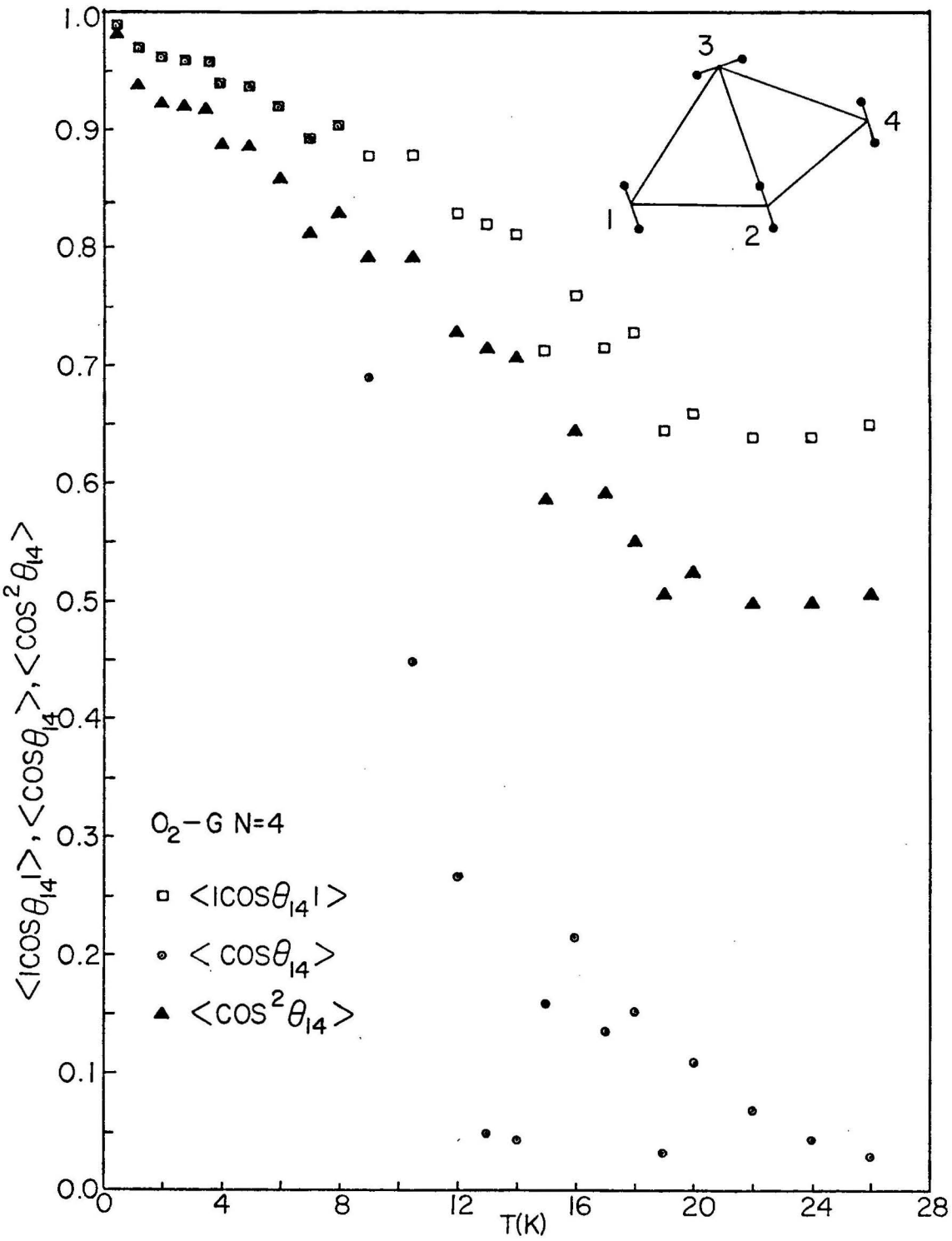

Figure IV-27. $\langle|\cos\theta_{14}|\rangle$, $\langle\cos\theta_{14}\rangle$, and $\langle\cos^2\theta_{14}\rangle$ in N = 4 δ-cluster.

Section IV-B-3, Melting and Dissociation Transitions

From both the average bond length and bond length fluctuation versus temperatures curves (Fig. IV-22), $T = 14$ K appears as a phase transition point for the $N = 3$ trimer. By examining some instantaneous structures along the Monte-Carlo Markov chain, it is found that the contour formed by connecting the positions of molecules 1, 2, and 3 in sequence alternate between being clockwise and counter-clockwise, when $T > 14$ K . While below 14 K , this phenomenon has not been observed. This indicates a structural breakdown at 14 K . We attribute this as a melting transition by comparison with melting transition in bulk systems.

Melting transitions for $N \geq 4$ are found by the same criteria for melting of β-clusters. Bond length fluctuations, average nearest neighbor distances, and the bond length histograms are properties we examine to detect the melting transition. The energy curves for $N = 7$ shows a gap between the crystallite state and fluid like state. For $N < 7$, however the energy increases with temperature smoothly without any indication of melting. In the energy versus temperature plot for $N = 7$ (Fig. IV-28), the points for $T = 15$ and 18 K fall onto the liquid phase curve, while the points for $T = 16$, 17, and 19 K fall onto the crystallite phase curve. The bond length analysis give the same information. The crystallite state and fluid like state coexist for $15 \text{ K} \leq T \leq 20 \text{ K}$. Similar phenomena exist for other cluster sizes.

The dissociation temperatures are defined in the same way as for the β-clusters. When the molecules move apart, the internal energy approaches to zero. The adsorption energy, however, does not change much because the molecules are still floating on the substrate.

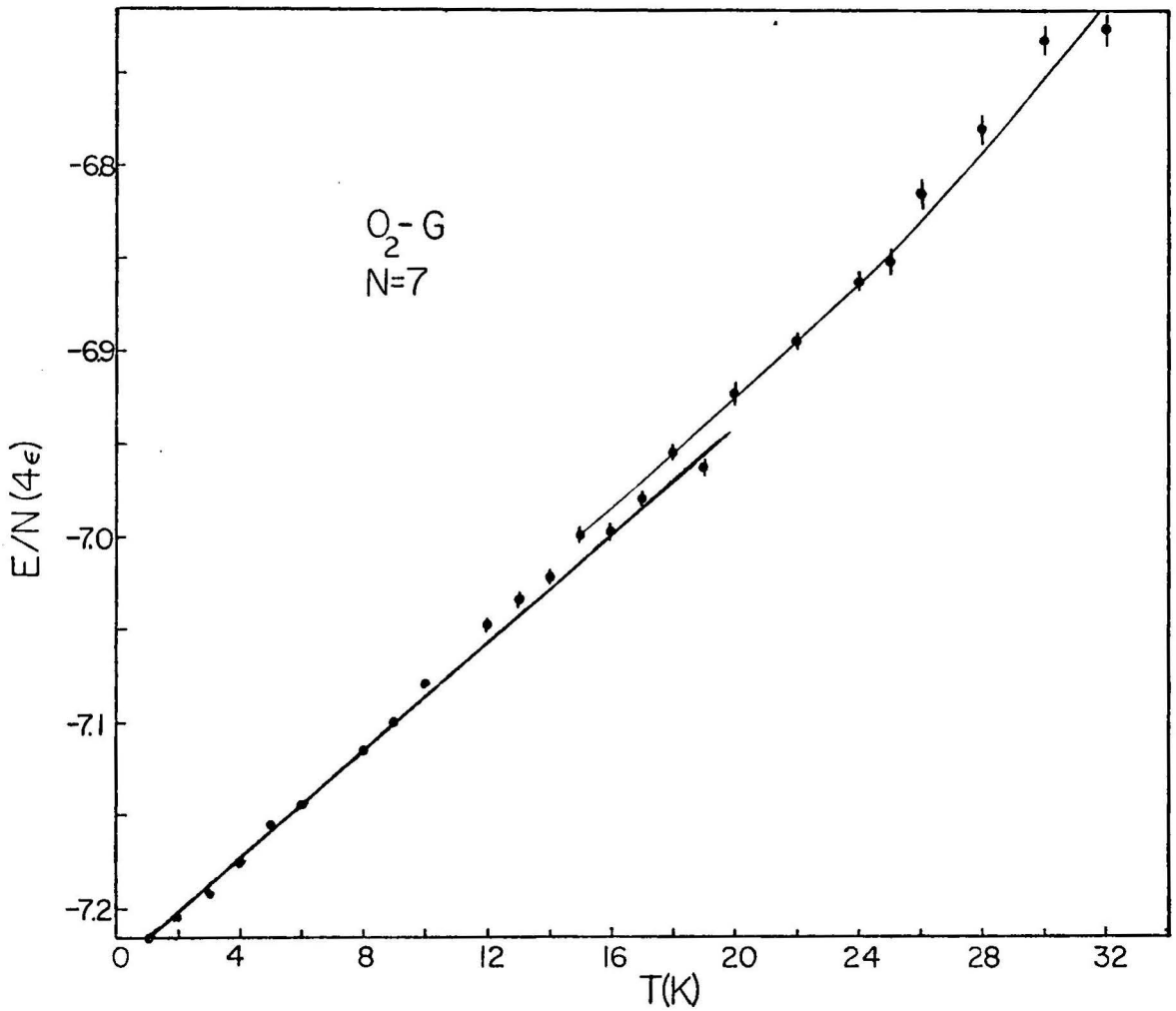

Figure IV-28. Total energy per molecule for N = 7 δ-cluster.

The melting temperatures and dissociation temperatures for all the cluster sizes and their uncertainties are plotted in Fig. IV-29.

Section IV-B-4, Summary

With an atom-atom potential for the oxygen-graphite interaction, all molecules in a cluster are parallel to the substrate surface. The structures are complicated by the orientations of the molecules. There are many isomers with similar center-of-mass structures but different molecular orientations. The $N = 3$ trimer shows a clear in-registry to out-of-registry transition. There are indications that this transition may exist for $N = 2$, 6, and 7 also. The $N = 5$ cluster has several isomers with energies very close to the ground state energy. The mixing of these energetically nearly degenerate states causes orientational disorder to occur at a very low temperature. Other sizes studied here all show orientational order-disorder transitions. All sizes except $N = 2$ exhibit melting transitions. Although melting transition is not found for $N = 3$ rare gas clusters[26] or β clusters, there is a quasi-melting phenomenon for the $N = 3$ δ clusters. This is attributed to the larger number of degrees of freedom associated with the structures, as discussed in this section. The melting temperatures and the dissociation temperatures for all cluster sizes studied are slightly lower than those for the β clusters. This is attributed to the lower internal binding strength in the δ clusters. We have carried out calculation of T_M for δ clusters for $N \leq 7$. This gives a prediction for melting temperature at $\rho < 0.2$, where available experimental result is limited.

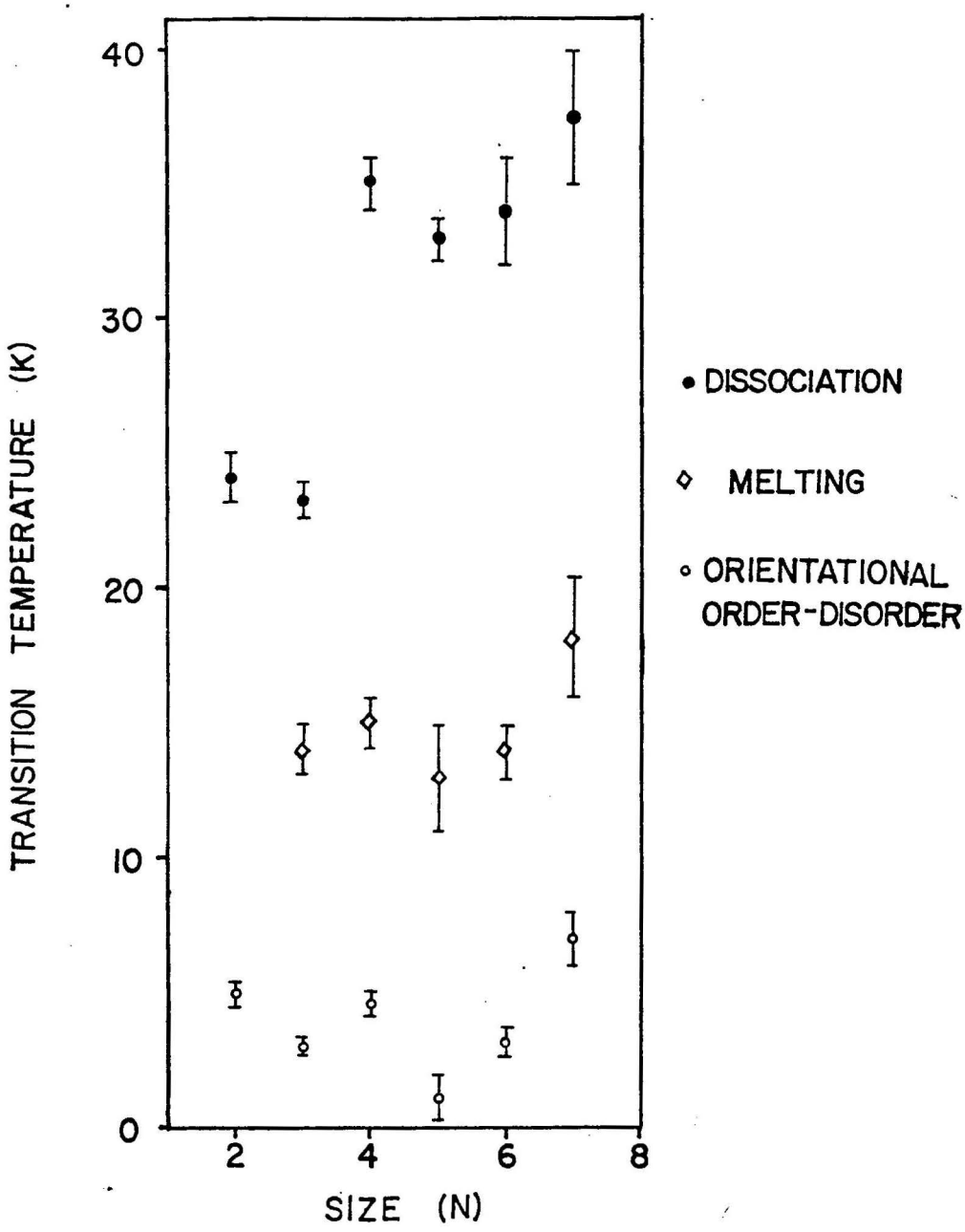

Figure IV-29. Transition temperature for δ-clusters.

Section IV-C, Adsorbed Infinite Monolayer Films

The structures and energies of adsorbed infinite oxygen film on graphite have been determined by an energy minimization scheme for various surface densities. A two sublattice structure with molecular centers sitting on a face centered rectangular lattice is assumed. The first sublattice consists of the molecules on the rectangular lattice points, while the second sublattice consists of the molecules on the centers of lattice rectangles. At a given film density, the lattice constant along one direction, the height of the film from graphite surface, and the molecular orientations of each sublattice are the independent variables used in the "pattern search" to find the minimal total energy. The equilibrium structure is determined by the values of these independent variables at the minimal energy point at each density investigated.

The averaged potential energy over the graphite surface without considering the surface structure (E_o only in Eq. II-16) is used to determine the adsorption energy. This is a proper approximation for an incommensurate film, which is found by our calculations and also confirmed by experiments. The internal energy of the film is determined by considering eighteen nearest neighbor oxygen molecules in the lattice sum. The total energy per unit surface area of the film as well as the adsorption energy per oxygen molecule is plotted as a function of film density in Fig. IV-30. The film coverage for a $\sqrt{3} \times \sqrt{3}$ commensurate (Fig. I-1) film is defined to be unity for convenience of comparison with results of other works. Two different surface interactions have been used. In the first case, the adsorption energy is obtained by summing the potential energies of the individual

oxygen atoms with the graphite. The dotted curve in Fig. IV-30 shows this adsorption energy per oxygen molecule (right-hand scale). The total energy, which is the adsorption energy plus the O_2 film internal energy, is given by the solid curve (left-hand scale). In the second case, the adsorption energy is calculated by assuming that each oxygen molecule interacts with graphite only through its center of mass. That is, O_2 - graphite anisotropies are neglected. The adsorption energy per oxygen molecule in this case is -4.9 for all coverages. The total energy per area is given by the dashed curve (left-hand scale).

With the isotropic O_2 - graphite interactions, the molecules are oriented perpendicular to the surface and sit on equilateral triangular sites for $\rho \geq 1.45$. When the coverage is decreased from $\rho = 1.45$, the molecules become tilted and the lattice becomes distorted from its original equilateral triangular structure. This can be understood by examining Fig. II-2, in which the intermolecular potential energy for a pair of oxygen molecules oriented with their molecular axes parallel, perpendicular, colinear with respect to each other, and forming a cross, are plotted versus the intermolecular distance R . With large R , corresponding to low coverage, the parallel structure no longer possesses the lowest pair energy and would not be the favored pair structure.

The absolute minimum for both the solid curve and the dashed curve in Fig. IV-30 occurs at $\rho = 1.81$, where the O_2 molecules sit on an equilateral-triangular lattice with their molecular axes perpendicular to the surface plane. However, a sharp change in the adsorption energy occurs at $\rho \approx 1.33$ when O_2 - graphite anisotropy is considered,

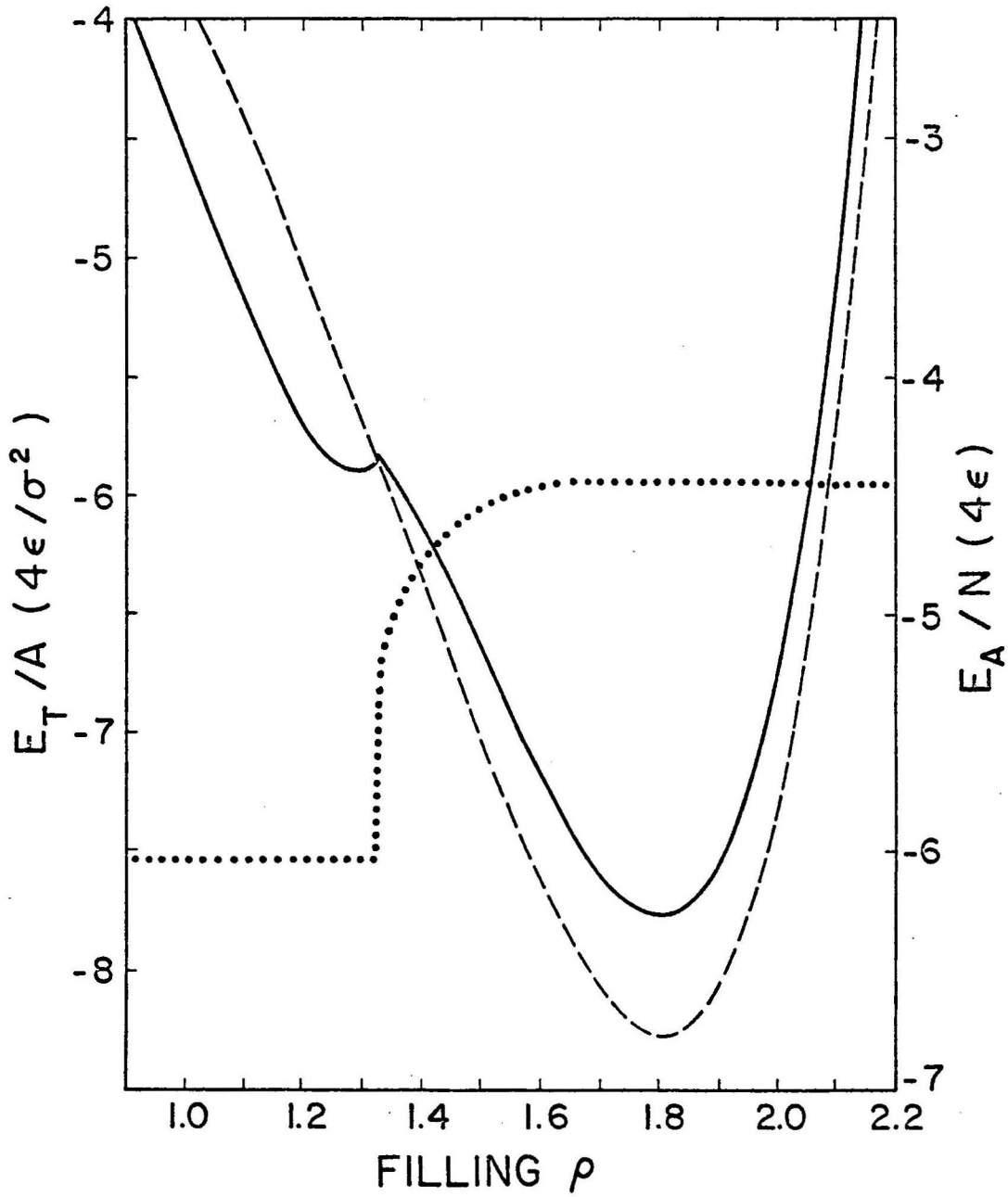

Figure IV-30. Energy per unit area of infinite monolayer films. Solid curve shows the total energy using an atom-atom potential for oxygen-graphite interaction. Dashed curve shows the energy using an isotropic oxygen-graphite interaction. The dotted curve shows the adsorption energy part (right hand scale) included in solid curve.

as in the first case. This change is accompanied by an orientational transition where the O_2 molecular axes become parallel to the substrate plane and to one another. The lattice is also distorted into that of isosceles triangles with the molecules at each vertex pointing along the perpendicular bisector. The sides of the triangle are 3.17 Å and 4.17 Å . The local minimum in the solid curve at $\rho \approx 1.3$ is actually the absolute minimum for the total potential energy per oxygen molecule. A comparison of the lattice configuration at $\rho = 1.30$ and $\rho = 1.81$ deduced from our calculations with that of Nielson and McTague's neutron diffraction studies[2] and the recent X-ray studies[10] is given in Fig. IV-31. The agreement is excellent.

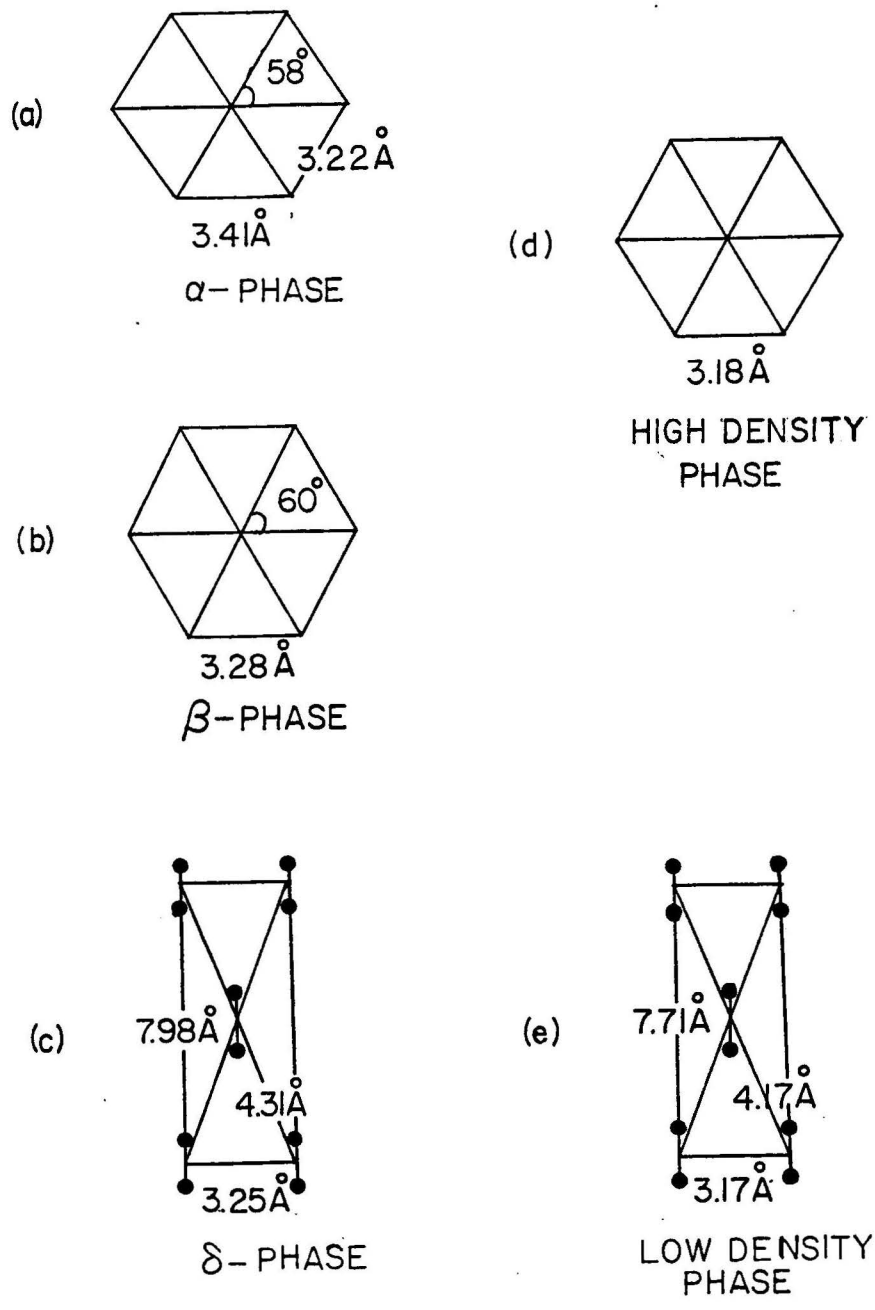

Figure IV-31. Film structures found by Neutron scattering (a,b), and X-ray scattering (c), and the structures found in this work (d,e) with an atom-atom potential for the oxygen-graphite interaction.

CHAPTER V

DISCUSSION AND CONCLUSION

Two different Monte-Carlo studies of adsorbed two-dimensional oxygen clusters on graphite have been carried out. In the first case, no surface interaction was included although the molecular centers are considered fixed on a plane. This approximation is similar to one in which an isotropic interaction between the O_2 and graphite is used, because the isotropic surface interaction keeps the molecular centers approximately on a plane above substrate. In this approximation, the $N = 2$ dimer has a crossed configuration and all other clusters have a structure in which the molecular axes are oriented perpendicular to the substrate plane. In a second approximation, the atom-atom Lennard-Jones potential is used to represent the oxygen-graphite interaction. In this case, each atom tends to stay at approximately the same distance from the graphite surface, so that the atoms in an adsorbed cluster are essentially planar, and oxygen molecular axes are parallel to the substrate. The molecular orientations with respect to graphite surface in these two approximations are similar to those in β and δ films, respectively. We call the clusters studied with the first approximation β clusters, and the clusters studied with the other approximation δ clusters.

For the β clusters, the orientational order-disorder transitions first appear as flipping of molecular axes between degenerate states. The orientational binding is stronger for the more tightly bound molecules in the cluster and as a result the interior molecules of the

$N = 6$ incomplete hexagon, $N = 7$, and $N = 12$ do not become orientationally disordered in the crystallite phase. The ideal free rotor states for O_2 are not observed until the cluster melts. For the δ clusters the orientational disorder first appears as a mixing of states of equivalent structures or isomeric states with different molecular orientations. After disordering the average bond length histogram becomes more sharply peaked showing the center-of-mass structures formed with equilateral triangles. Most of the molecules become nearly planar free rotor states prior melting.

The melting of the adsorbed two-dimensional cluster is not as well-defined as for three-dimensional rare gas clusters. The discontinuities in their energies are small and Van der Waal's loops appear to exist. Other workers have reported similar results in two-dimensional systems.[29] Melting phenomena in two-dimensional films differ considerably from the three-dimensional bulk systems.[30] A two-dimensional film loses lattice order gradually from longer range to shorter range as the temperature increases. Theories about a continuous melting transition range bounded by two second-order transitions have been suggested for some adsorbed films.[31] For given size N, the melting temperature for β clusters are higher than that for δ clusters.

The δ clusters dissociate at lower temperatures than β clusters, However, the differences are not as large as for melting temperatures.

The lattice structures and energies for infinite films adsorbed on graphite have been studied with an energy minimization technique. There are two minima in the energy per unit area with respect to film density curve, when a atom-atom Lennard-Jones potential is used to

represent the interaction between oxygen and graphite. The lower density minimum gives a structure corresponding to the measured δ phase film.[10] The nearest neighbor distances at this minimum are 3.17 Å and 4.17 Å, which are 3% less than measured values, 3.25 Å and 3.14 Å.[10] The higher density minimum corresponds to the β phase film with nearest neighbor distance 3.18 Å, which also agrees with the measured distance 3.28 Å[2] to 3%. If the anisotrophy of the oxygen-graphite interaction is ignored, i.e., if the oxygen molecule interacts with graphite through its center of mass, only one energy minimum exists. Comparing with the available data, results using atom-atom surface interaction seem to be in the best agreement with experiment.

At $\rho \simeq 1$, the film is in an isosceles triangular structure with about 30% difference in nearest neighbor bonds. It would be necessary to raise the energy very much to bring this film into a triangular lattice to be commensurate with the graphite lattice. Therefore, we predict that it is very unlikely to form the commensurate film at $\rho \simeq 1$.

At extreme low coverage, the amount of adsorbed oxygen is far below that required to form a complete film and the system properties may be understood using a cluster model. With the oxygen-graphite interaction used for δ-cluster studies, we are able to predict the equilibrium configurations of the low density phase in excellent agreement with experiments. It also becomes possible for us to estimate the melting temperature, T_M, of the low temperature phase.

The β clusters, with their molecular orientations perpendicular to the substrate, are analogous to the higher density film, the

β-phase film. Extrapolation of the melting temperatures for β clusters allow us to predict the melting temperature of the β-film. It is also found that the interior molecules in the β-cluters do not undergo orientational transitions prior to melting while all edge molecules do. This provides useful information on defects and vacancies in the β-phase infinite film. Understanding of the physical properties of these clusters may then suggest methods for investigation of the higher density film, such as the density of vacancies and shapes and propagation of defects.

REFERENCES

1. J. K. Kjems, L. Passell, H. Taub, J. G. Dash, and A. D. Novaco. Phys. Rev. B 13 (4):1446(1976).

2. M. Nielsen, J. P. McTague. Phys. Rev. B 19 (6):3096(1979).

3. P. W. Stephens, P. Heiney, and R. J. Birgeneau, and P. M. Horn. Phys. Rev. Lett. 43 (1):47(1979).

4. H. Shiba. J. Phys. Soc. Jap. 46 (6):1852(1979).

5. C. G. Shaw, S. C. Fain, Jr., and M. D. Chinn. Phys. Rev. Lett. 41 (14):955(1978).

6. A. D. Novaco and J. P. McTague. J. Phys. (Paris) Colloq. 38 (C4):116(1977).

7. C. Fuselier. Ph.D. dissertation, Colorado State University, 1979.

8. R. Marx and R. Braun. Solid State Comm. 33 :229(1980), Proc. 4th Int. Conf. on Solid State Surfaces and the 3rd European Conf. on Surface Science, Sept. 22 - Sept. 26, 1980, pp. 100-103.

9. J. Stoltenberg and O. E. Vilches. Phys. Rev. B 22 (6):2920(1980).

10. R. W. Stephens, P. A. Heiney, R. J. Birgeneau, P. M. Horn, J. Stoltenberg, and O. E. Vilches. Phys. Rev. Lett., to be published.

11. J. Frenkel. Theory of Liquids, Dover, New York, 1955.

12. J. Farges, M. F. DeFerauday, B. Raoult, and G. Torchet. J. Phys. (Paris) Colloq. 36 :C2-13(1975).

13. (a) S. W. Marshall and R. M. Wilenzick. Phys. Rev. Lett. 16 : 219(1966).

    (b) R. Kubo. J. Phys. Soc. Jap. 17 :975(1962).

    (c) J. M. Dickey and A. Paskin. Phys. Rev. Lett. 21 :1441(1968).

    Phys. Rev. B 1 :851(1970).

    (d) B. G. Bagley, Nature 208 :674(1965), ibid. 225 :1040(1970).

14. J. A. Venables and D. J. Ball. Proc. Roy. Soc. Lond. A322 :331 (1971).

15. M. Weissmann and N. V. Cohan. J. Chem. Phys. 72 :4562(1980).

16. C. A. English and J. A. Venables. Proc. Roy. Soc. A340 :57(1974).

17. M. F. Collins. Proc. Phys. Soc. 89 :415(1966).

18. C. A. English and J. A. Venables. Proc. Roy. Soc. (London) A 340: 81(1974).

19. W. A. Steele. Surface Science 36 :317(1973).

20. W. A. Steele. J. Phys. (Paris) Coloq. 38: C4-61(1977).

21. C. R. Fuselier, N. S. Gillis, and J. C. Raich. Solid State Comm. 25 :747(1978).

22. J. Eckert, W. D. Ellenson, J. B. Hastings, and L. Passell. Phys. Rev. Lett. 43 (18):1329(1979).

23. T. H. Spurling and E. A. Mason. J. Chem. Phys. 46 (1):322(1967).

24. J. J. Hammersley and D. C. Handscomb. Monte Carlo Methods, Methuen, London, 1964.

25. N. Metropolis, A. Rosenbluth, M. Rosenbluth, A. Teller, and E. Teller. J. Chem. Phys. 21 :1087(1953).

26. (a) R. D. Etters and J. B. Kaelberer. Phys. Rev. A 11 :1068(1975).

    (b) J. B. Kaelberer and R. D. Etters. J. Chem. Phys. 66 :5112 (1977).

    (c) J. B. Kaelberer, Ph.D. dissertation, Colorado State University, 1975.

27. D. J. Wilde and C. S. Brightler. Foundations of Optimization, Prentice-Hall, Englewood Cliffs, N.J., 1967.

28. (a) F. Lindemann. Phys. Z. 11 :609(1910).

    (b) D. Pines. Elementary Excitations in Solids, Benjamin, New York, 1964.

29. F. Van Swol, L. V. Woolcock, and J. N. Cape. J. Chem. Phys. 73 (2):913(1980).

30. J. G. Dash. Films on Solid Surfaces, Academic Press, New York, 1975.

31. (a) B. I. Halperin and D. R. Nelson. Phys. Rev. Lett. 41 :121 (1978).

    (b) D. Frenkel and J. P. McTague. Phys. Rev. Lett. 42, 1632(1979).